A miR-124-mediated post-transcriptional mechanism controlling the cell fate switch of astrocytes to induced-neurons

Elsa Papadimitriou[1], Paraskevi N. Koutsoudaki[1,&], Timokratis Karamitros[2,#], Dimitra Karagkouni[3,#], Dafni Chroni-Tzartou[4], Christos Gkemisis[1], Maria Margariti[1], Evangelia Xingi[5], Irini Thanou[1], Socrates J. Tzartos[4], Artemis G. Hatzigeorgiou[3], Dimitra Thomaidou[1,5,*]

Affiliations

[1]Neural Stem Cells and Neuro-imaging Group, Department of Neurobiology, Hellenic Pasteur Institute

[2]Bioinformatics and Applied Genomics Unit, Department of Microbiology, Hellenic Pasteur Institute

[3]DIANA-Lab, Hellenic Pasteur Institute & Dept. of Computer Science and Biomedical Informatics, Univ. of Thessaly

[4]Laboratory of Molecular Neurobiology and Immunology, Department of Neurobiology, Hellenic Pasteur Institute

[5]Light Microscopy Unit, Hellenic Pasteur Institute

[#]equally contributing authors

[&]Present address: Molecular Carcinogenesis Group, Department of Histology and Embryology, Medical School, National and Kapodistrian University of Athens, Athens, Greece

[*] Corresponding author

Email: thomaidou@pasteur.gr

Abstract

miRNA miR-124 has been employed supplementary to neurogenic TFs and other miRNAs to enhance direct neurogenic conversion by suppressing multiple non-neuronal targets. Aim of the study was to investigate whether miR-124 is sufficient to drive direct reprogramming of astrocytes to induced-neurons (iNs) on its own and elucidate its independent mechanism of reprogramming action. Our data show that miR-124 is a potent driver of the reprogramming switch of astrocytes towards an immature neuronal fate by directly targeting the RNA-binding protein Zfp36l1 and subsequently de-repressing Zfp36l1 neurogenic interactome. To this end miR-124 contribution in iNs production largely recapitulates endogenous neurogenesis pathways, being further enhanced upon addition of the neurogenic compound ISX9, which greatly improves both miR-124-induced reprogramming efficiency and iNs' functional maturation. Importantly, miR-124 is potent to guide direct neuronal reprogramming of reactive astrocytes to iNs of cortical identity *in vivo* following cortical trauma, a novel finding confirming its robust reprogramming action under neuroinflammatory conditions.

Introduction

Direct astrocytic reprogramming to induced-neurons (iNs) is a powerful approach for manipulating cell fate, as it takes advantage of the intrinsic neural stem cell (NSC) potential of reactive astrocytes (Magnusson et al. 2014), while it offers the possibility of reprogramming resident brain cells. To this end astrocytic cell fate conversion to iNs has been well-established in vitro (Berninger et al. 2007; Heinrich et al. 2010; Aravantinou-Fatorou et al. 2015) and in vivo (Guo et al. 2014; Torper et al. 2013; Mattugini et al. 2019) using combinations of transcription factors (TFs) or chemical cocktails (L. Zhang et al. 2015; Xiang Li et al. 2015; Gao et al. 2017). Challenging the expression of lineage-specific TFs during reprogramming is accompanied by changes in the expression of regulatory RNAs, mostly miRNAs, that post-transcriptionally modulate high numbers of neurogenesis-promoting factors, indicating that miRNAs act as key regulators of cell fate conversion (Xuekun Li and Jin 2010). To this end, miRNAs have been introduced, supplementary or alternatively to TFs, to instruct direct neuronal reprogramming (Yoo et al. 2011).

Among neurogenic miRNAs, miR-124 has been shown to contribute to efficient neurogenic conversion of fibroblasts when coupled with certain TFs or other miRNAs, in particular miR-9/9*,and the strong neuronal reprogramming potential of this cocktail has been elaborately studied at the transcriptomic and epigenetic level (Ambasudhan et al. 2011; Abernathy et al. 2017; Wohl and Reh 2016; Victor et al. 2014). miR-124 is the most abundant miRNA in the CNS, participating both in embryonic (Maiorano and Mallamaci 2009) and adult neurogenesis (Cheng et al. 2009; Åkerblom et al. 2012), while its expression persists in mature neurons (Deo et al. 2006). miR-124 acts globally to increase the expression levels of neuronal genes, by repressing components of major neuronal gene repressor complexes, such as the anti-neural transcriptional repressor REST complex (Visvanathan et al. 2007; Baudet et al. 2012; Volvert et al. 2014) and the Polycomb Repressive Complex 2 (PRC2) (Neo et al. 2014; S. W. Lee et al. 2018), while it also participates at the post-transcriptional regulation of neuronal transcripts by targeting the neuron-specific splicing global repressor Ptbp1 (Makeyev et al. 2007). Besides its roles in transcriptional and post-transcriptional regulation, miR-124 neurogenic action also relates to chromatin dynamics, as it acts as a key mediator of a chromatin permissive environment for neuronal reprogramming through its involvement in the formation of the neuron specific chromatin remodeling complex nBAF (Yoo et al. 2009).

However, although miR-124 has been lately utilized in many reprogramming cocktails for the neurogenic conversion of fibroblasts (Ambasudhan et al. 2011; Birtele et al. 2019; Jiang et al.

84 2015; Victor et al. 2018; Yoo et al. 2011), neither its potential to induce fate conversion of
85 astrocytes to iNs *in vitro* or *in vivo*, nor its mechanism of action in instructing direct
86 reprogramming on its own have been investigated. In this study we show that miR-124 is
87 sufficient to instruct reprogramming of cortical astrocytes to immature induced-neurons (iNs)
88 *in vitro* controlling the reprogramming "switch" of astrocytes towards the neuronal fate by
89 down-regulating genes with important regulatory roles in astrocytic function. Among these
90 we identified for the first time the RNA binding protein Zfp36l1, implicated in ARE-mediated
91 mRNA decay (Lai et al. 2000), as a direct target of miR-124 and further found certain neuronal-
92 specific Zfp36l1targets that participate in cortical development being de-repressed in miR-
93 124-iNs, implying that miR-124-induced reprogramming recapitulates pathways of
94 endogenous cortical neurogenesis. Importantly, by blocking miR-124 specific binding in
95 Zfp36l1 3'UTR, we revealed that miR-124/Zfp36l1 interaction is one of the drivers of miR-124-
96 induced astrocytic cell fate switch and induction of neuronal identity. To enhance the
97 neuronal differentiation of reprogrammed immature iNs, we combined miR-124 with
98 isoexasole-9 (ISX9) chemical compound known to possess neurogenesis-promoting properties
99 (Schneider et al. 2008; Xiang Li et al. 2015). Our functional and mechanistic analysis of the two
100 molecules combination revealed that in vitro addition of ISX9 promoted both the neurogenic
101 conversion and greatly enhanced the functional maturation of miR-124+ISX9-iNs reinforcing
102 their passage through a Tbr2+ intermediate stage. Importantly, *in vivo* miR-124 was also
103 potent either alone or along with ISX9, to guide neuronal reprogramming of reactive
104 astrocytes to iNs following cortical trauma, with the vast majority of iNs exhibiting deep-layer
105 cortical identity, implying the strong miR-124 reprogramming capacity within the injured brain
106 micro-environment.

107 # Results

108 **miR-124 is sufficient to instruct reprogramming of postnatal cortical astrocytes to immature**
109 **induced- neurons (immature-iNs)**

110 In order to study the potential of miR-124 to instruct neuronal reprogramming of astrocytes
111 on its own, cultured postnatal day3-5 (P3-5) mouse cortical astrocytes were transfected with
112 the miR-124-3p mimic 3 times every two days and were supplemented with the antioxidants
113 vitamin E and ascorbic acid (**Fig.1A**). After 1 week (day7) nearly 35% of miR-124 over-
114 expressing cells in culture were Tuj1+ exhibiting multipolar morphology **(Fig.1B,C)**, as
115 compared to control astrocytes that received scrambled miRNA (sc-miRNA) (**Suppl.Fig.1A**),
116 where no Tuj1positivity was detected. Still, miR-124-iNs exhibited low differentiation
117 potential and only 19% of the cells remained Tuj1+ at day14 of the reprogramming protocol
118 (**Fig.1B, C**). The ability of miR-124 to instruct neurogenic reprogramming was further
119 supported by RT-qPCR expression analysis of several neurogenic transcription factors (TFs) at
120 day7, where miR-124 overexpression induced the up-regulation of the mRNA levels of the
121 proneural bHLH TFs *Mash1* and to a lesser extend *Neurog2* (**Fig.1D**), while it additionally up-
122 regulated TFs related to both dorsal (*Tbr2, Tbr1, Fezf2* and *Cux1*) (**Fig.1E**) and ventral
123 telencephalon development (*Gsx2, Dlx1*) (**Fig.1F**). We also observed up-regulation of TFs
124 related to neuronal differentiation (*Sox4, Sox11, Hes6*) (**Fig.1G**), however we failed to detect
125 an up-regulation of *NeuroD1* (**Fig.1G**), which is known to play a crucial role in neuronal
126 reprogramming (Pataskar et al. 2016; Guo et al. 2014; Matsuda et al. 2019). Instead, miR-124
127 significantly reduced *NeuroD1* mRNA levels, implying that this reduction may contribute to
128 the low differentiation capacity of miR-124-iNs. Further, immunofluorescence analysis
129 indicated that the majority of miR-124-iNs (nearly 80%) were Mash1+ and also exhibited low
130 Tbr2 expression (nearly 70%), while only a small percentage of reprogrammed cells (15%)
131 were positive for the ventral TF Gsx2 (**Fig.1H, I**), indicating that the Mash1-Tbr2 trajectory is
132 most prominently activated in the majority of miR-124-iNs.

133 **The neurogenic compound ISX9 greatly enhances the miR-124-induced reprogramming**
134 **efficiency and differentiation state of iNs**

135 The observed down-regulation of NeuroD1 by miR-124 prompted us to supplement the
136 reprogramming medium from day2 to day10 with the chemical compound ISX9, known to up-
137 regulate NeuroD1 levels and enhance neuronal differentiation (Schneider et al. 2008). Indeed,
138 the addition of ISX9 led to the acquisition of a more differentiated neuronal-like phenotype

139 with a smaller soma and longer projections (**Fig.2A**) and significantly increased the percentage
140 of Tuj1+ reprogrammed cells to 62% at day7, with an average of 38% of them being detected
141 at day14 (**Fig.2B**). Importantly, ISX9 was potent to reverse the miR-124-induced reduction of
142 NeuroD1 mRNA levels (**Fig.2C**) and to greatly elevate the transcriptional levels of *Neurog2* and
143 *Tbr2* peaking at day7 (**Fig.2D**), while it also induced a moderate reduction in the mRNA levels
144 of *Mash1* (**Fig.2E**). Interestingly, ISX9 was not able to induce reprogramming of astrocytes on
145 its own (sc-miRNA+ISX9) (**Suppl.Fig.1B**), despite evoking robust up-regulation of the mRNA
146 levels of *NeuroD1* (**Fig.2D**) and other neurogenic TFs (**Suppl.Fig.1C**) and to a small, but
147 significant, extend the protein levels of Mash1 and Tbr2 (**Suppl.Fig.1D, E**). However, addition
148 of ISX9 in the reprogramming medium along with miR-124 significantly increased the
149 percentage of Tbr2+/Tuj1+ iNs, without significantly affecting either the percentage of
150 Mash1+/Tuj1+ iNs or Gsx2+/Tuj1+ iNs relative to miR-124 alone (**Fig.2F, G**). Quantification of
151 the protein levels of Mash1 and Tbr2 by measuring their mean nuclear fluorescence intensity
152 in miR-124-iNs and miR-124+ISX9-iNs at day7, revealed a significant enhancement of Tbr2
153 protein levels (**Fig.2H**) and a down-regulation of Mash1 levels (**Fig.2I**) following ISX9 addition.

154 These results led us to the inference that addition of ISX9 in the reprogramming medium
155 reinforces the passage of miR-124+ISX9-iNs through a Tbr2+ intermediate stage, which seems
156 to be the main reprogramming route these iNs follow. Interestingly, the addition of ISX9 also
157 significantly enhanced the expression of *Insm1* (**Suppl.Fig.1F**), a key transcriptional regulator
158 of intermediate progenitors (IPs) (Elsen et al. 2018), further supporting the notion that iNs
159 pass through an intermediate stage bearing molecular characteristics of endogenous IPs.

160 **miR-124+ISX9-iNs exhibit characteristics of mature, electrophysiologically active neurons**

161 The majority of miR-124-iNs and miR-124+ISX9-iNs were positive for the cortical deep-layer
162 TF Tbr1 at day14 (**Suppl.Fig.2A, B**). We mainly observed a moderate nuclear Tbr1 expression
163 in miR-124-iNs, whereas miR-124+ISX9-iNs exhibited strong cytoplasmic Tbr1 expression,
164 besides a moderate nuclear one (**Suppl.Fig.2A**). After 21 days in culture, nearly 80% of Tuj1+
165 miR-124+ISX9-iNs were also positive for the mature neuronal markers MAP2 and Synapsin1,
166 exhibiting a differentiated neuronal morphology (**Fig3.A,B**), while miR-124-iNs at day21 did
167 not exhibit signs of further maturation and only a small percentage of them were positive for
168 MAP2 and Synapsin1 (**Fig.3B**). Additionally, at day28 the majority of miR-124+ISX9-iNs (nearly
169 90%) were positive for the glutamatergic marker vGlut1 (**Fig.3C, D**), while only 12% of them
170 were found positive for GABA (**Fig.3D, Suppl.Fig.2C**).

171 In order to further establish the functional maturation state of miR-124-iNs and miR-
172 124+ISX9-iNs we performed electrophysiological analysis with whole-cell voltage-clamp and
173 current-clamp recordings at different time points from day15 to day27. Rapidly inactivating
174 inward Na^+ currents and persistent outward K^+ currents were recorded in miR-124+ISX9-iNs
175 after 22 days in culture (n=47 out of 80 analyzed cells) in response to depolarizing voltage
176 steps (**Fig.3E, left panel, Fig. 3F**), while further application of TTX and TEA – selective Na^+
177 channels' (Na_V) and K^+ channels' (K_V) blockers respectively – confirmed that the Na_V were
178 responsible for the inward currents and K_V for the outward currents (**Fig.3E, middle and right**
179 **panels**). A small amount of K_V channels started being present in miR-124+ISX9-iNs before
180 day21, while they became more evident in days 23-27 **(Fig.3F)**, in accordance with the ability
181 of almost all recorded miR-124+ISX9-iNs (n=21 out of 30 recorded cells) to generate repetitive
182 action potentials (APs) upon membrane depolarization (**Fig.3G**). Finally, rare spontaneous
183 post-synaptic current activity was detected in few mature miR-124+ISX9-iNs (day27) (**Fig.3H**).
184 On the other hand, miR-124-iNs exhibited lower amounts of Na_v and K_v channels (not shown)
185 and thus were not capable of firing action potentials (APs) (n=15 cells).

186 The majority (80%) of miR-124+ISX9-iNs (**Fig.3I**) and a few miR-124-iNs (not shown) were
187 capable of responding to different concentrations of GABA early in the course of their
188 maturation (day22), even before the appearance of APs, which is in compliance with the
189 expression of GABA receptors in early stages of neuronal development (Luján, Shigemoto, and
190 López-Bendito 2005). Additionally, miR-124+ISX9-iNs were capable of responding to L-
191 glutamate in a concentration dependent manner (**Fig.3J**), while L-glutamate-sensitive inward
192 current was completely blocked after co-application of 100μM L-glutamate and 20μM CNQX,
193 indicating the presence of AMPA/kainite receptors (**Fig.3K**).

194 **miR-124 and ISX9 exhibit both independent and cooperative transcriptional contributions**
195 **in the reprogramming process to iNs**

196 To in-depth analyze the molecular mechanism through which miR-124 contributes to the
197 reprogramming process either alone or following ISX9 supplementation, we performed RNA-
198 sequencing of miR-124-iNs and miR-124+ISX9-iNs at day7, using as controls astrocytes
199 obtained the initial day of the reprogramming (day1) and sc-miRNA transfected astrocytes at
200 day7. The differential expression analysis was performed between day7 miR-124-iNs or miR-
201 124+ISX9-iNs and day1 astrocytes (astro) (miR-124-iNs vs astro and miR-124+ISX9-iNs vs astro
202 respectively), whereas the day7 sc-miRNA-transfected astrocytes (sc-miRNA astro) were used
203 as the ultimate control for the analysis of miR-124 target genes (see Fig.5 below). We

204 identified 4,233 differentially expressed genes (DEGs) in miR-124-iNs vs astro and 6,652 DEGs
205 in miR-124+ISX9-iNs vs astro ($1 \leq \log_2$(fold change)≤ -1, FDR<0.05) (**Suppl.Fig.3A**).

206 Heat map analysis of DEGs (miR-124-iNs vs astro and miR-124+ISX9-iNs vs astro) that belonged
207 to the GO terms: Glial cell differentiation, Gliogenesis, Astrocyte development, Generation of
208 neurons, Neuron differentiation, Regulation of neuron differentiation, Neurotransmitter
209 transport and Synaptic signaling (**Fig.4A**) indicated that miR-124 alone efficiently down-
210 regulated a gene cluster enriched in astrocytic genes (**Cluster I**), with a small additional
211 contribution from ISX9. At the same time miR-124 up-regulated a gene cluster of neuronal
212 specific genes (**Cluster III**) that was to a large extend further up-regulated by ISX9
213 supplementation, while ISX9 highly up-regulated a neuronal specific gene cluster (**Cluster II**)
214 that was most exclusively expressed in miR-124+ISX9-iNs.

215 GO enrichment analysis of biological processes for the up-regulated DEGs of both miR-124-
216 iNs vs astro and miR-124+ISX9-iNs vs astro, further revealed that miR-124 alone up-regulated
217 genes related to generation of neurons and neuron differentiation as well as to more specific
218 neuronal functions mostly associated to synaptic transmission (**Fig.4B in orange**), while the
219 addition of ISX9 greatly enhanced the number of up-regulated genes related not only to
220 similar GO terms up-regulated by miR-124, but also to more mature neuronal functions such
221 as action potential, axon development and subtype specific synaptic transmission (**Fig.4B in**
222 **red**). Furthermore, enrichment analysis of the down-regulated DEGs of miR-124-iNs vs astro
223 indicated that many of them were related to cell cycle, gliogenesis, and astrocyte
224 differentiation (**Fig.4C**). Interestingly, this analysis revealed a strong effect of miR-124 in
225 down-regulating components of many signaling pathways, including MAPK, PKB, canonical
226 Wnt, TGF-β, BMP, Notch and JAK/Stat signaling pathways (**Fig.4C**), known to play important
227 roles in astrocytic identity and function (Gross et al. 1996; Acaz-Fonseca et al. 2019; Kang and
228 Hébert 2011; Yang et al. 2012).

229 Since reprogramming is a process that implicates great changes in the transcriptomic, post-
230 transcriptomic and epigenetic landscape of trans-differentiating cells, we sought to identify
231 the differentially expressed transcription factors (TFs), epigenetic factors (EFs) and RNA
232 binding proteins (RBPs) in our datasets that could possibly drive the reprogramming process.
233 Heat map analysis of astrocytic TFs (**Suppl.Fig.3B**) indicated that miR-124 alone potently
234 down-regulated TFs related to astrocytic function such as *Id1, Id3, Tcf4, Tcf7l1, Rbpj, Nfic,*
235 *Zcchc24, Pparg, Nr3c1* and *Tead1*, while the addition of ISX9 exhibited only a small
236 contribution to their down-regulation (**Suppl.Fig.3B**). Importantly, validation of many of those
237 genes with RT-qPCR verified the observed trend and also indicated that ISX9 alone (sc-

238 miRNA+ISX9) failed to down-regulate their mRNA levels (**Suppl.Fig.3C**). In parallel, heat map
239 analysis of up-regulated neuronal-specific TFs revealed that miR-124 led to the up-regulation
240 of TFs related to telencephalon development such as *Tox, Foxo6, Scrt1, Scrt2, Rcor2, Rarb,*
241 *Rxrg, Dlx5* and *Sox21* (**Fig.4D**), along with TFs that we had already identified through prior RT-
242 qPCR analysis (*Mash1, Insm1, Hes6, Sox4, Fezf2, Gsx2, Dlx1*). Additionally, the
243 supplementation with ISX9 increased the number of TFs implicated in telencephalon
244 development, among which *Eomes (Tbr2), Prdm8, Ovol2, Tfap2c, Tshz2, Lhx6* and *Cux2*
245 (**Fig.4D**). Surprisingly, we identified a rather large set of TFs highly up-regulated only following
246 ISX9 addition, related to more ventral/caudal brain regions than the telencephalon, such as
247 the retina, midbrain, hindbrain/spinal cord (**Fig.4D**), a finding posing the possibility that ISX9
248 expands region-specific neuronal identity at least at the transcriptional level. Validation of
249 selected TFs/EFs expressed either in telencephalon (**Suppl.Fig.3D**) or in midbrain
250 (**Suppl.Fig.3E**) and hindbrain/spinal cord (**Suppl.Fig.3F**) by RT-qPCR verified their observed up-
251 regulation by the addition of ISX9.

252 Interestingly, heat map analysis of differentially expressed RNA-binding proteins (RBPs)
253 revealed that miR-124 was sufficient to down-regulate many RBPs expressed in astrocytes and
254 other non-neuronal cells, such as the splicing factors *Ptbp1, Snrpa1, Lgals3, Isy1, Ddx39* and
255 *Syf2*, as well as the mRNA decay proteins *Zfp36, Zfp36l1, Zfp36l2* (**Fig.4E**). In addition, miR-124
256 moderately up-regulated several neuronal specific RBPs, mostly relevant to mRNA splicing and
257 stabilization, among which *Elavl2, Elavl4, Nova1, Rbfox1, Rbfox2, Celf3, Nol3, Nol4* and
258 *Adarb1*, while the addition of ISX9 induced further up-regulation of their mRNA levels and
259 significantly increased the number of genes implicated in neuron specific splicing, editing or
260 translation such as *Aplp1, Celf4, Celf5, Celf6, Elavl3, Ern2, Esrp2, Rbfox3, Rbm11, Ssrm4* and
261 *Tdrd6* (**Fig.4E**).

262 The analysis of differentially expressed EFs revealed that miR-124 increased on its own the
263 levels of several EFs related to epigenetic transcriptional activation, including the H3K4
264 methyltransferase *Kmt2c*, the DNA demethylase *Tet1*, the chromatin remodeling factors
265 Smarca1, Smarca2, Chd7, as well as the neuronal BAF (nBAF) complex component *Ss18l1*
266 *(Crest)* (**Suppl.Fig.4G**). On the other hand ISX9 further contributed in up-regulating the brain
267 specific chromatin remodeling factor Chd5, the nBAF complex components *Actl6b* and *Dpf3*
268 and the H3K4 methyltransferase *Smyd3*, while interestingly it majorly contributed in down-
269 regulating EFs related to epigenetic transcriptional repression, such as the H3K9
270 methyltransferases *Suv39h1* and *Suv39h2*, the histone deacetylases *Hdac5* and *Hdac7*, the

271 components of repressor complexes *Cbx5, Sap18* and *Rbbp4*, and the component of non-
272 neuronal BAF complexes *Dpf2* (**Suppl.Fig.4G**).

273 The above observations led us to the conclusion that miR-124 over-expression is sufficient to
274 induce the astrocytic reprogramming switch towards an immature cortical neuronal fate
275 through down-regulation of many glial specific genes, many of which are implicated in
276 different regulatory levels, such as the transcriptional, post-transcriptional, epigenetic and
277 signaling pathway level. The addition of ISX9, on the other hand, acts auxiliary to miR-124
278 reprogramming action enhancing neuronal-specific gene transcription contributing to the
279 maturation of miR-124 immature-iNs.

280 **The non-neuronal RBP Zfp36l1 is a novel direct target of miR-124**

281 To get a closer insight into the post-transcriptional effects of miR-124 on the astrocytic
282 transcriptome, we sought to determine the direct targets of miR-124 that could act as drivers
283 of the reprogramming switch. Argonaute (AGO) HITS-CLIP experiments are considered the
284 avant-garde of high-throughput methodologies for the direct detection of miRNA targets on
285 a transcriptome-wide scale. Therefore, we utilized publicly available AGO-HITS-CLIP data,
286 performed in mouse brain cortex (Chi et al. 2009) in order to detect miR-124 binding sites.
287 The analysis revealed 171 miR-124 direct targets that were also defined as down-regulated in
288 the miR-124-iNs vs sc-miRNA astro RNA-Seq analysis ($\log_2$(fold change)≤-1, FDR<0.01). miR-
289 124 targets were subsequently filtered to examine genes expressed in astrocytes, utilizing a
290 published reference list for expressed transcripts in distinct cell types of the mouse brain (Y.
291 Zhang et al. 2014), ending up with 130 miR-124 direct target genes (**Fig.5A**).

292 Among these genes, a prominent target was the RBP Zfp36l1, which is implicated in the mRNA
293 decay (Lai et al. 2000) and is highly expressed in cortical glial cells (Weng et al. 2019), cortical
294 radial glial precursors (Yuzwa et al. 2017; Weng et al. 2019) and other non-neuronal cells
295 (Carrick and Blackshear 2007). miR-124 directly binds to the 3' UTR of Zfp36l1 transcript with
296 perfect seed complementarity (7mer-M8 site) (**Fig.5B**), while in re-analysis of publicly
297 available AGO-HITS-CLIP data from human motor cortex and cingulate gyrus tissues, the miR-
298 124 binding site on the 3' UTR of ZFP36L1 human transcript was found to be conserved
299 (**Fig.5B**).

300 The efficient down-regulation of *Zfp36l1* by miR-124 was validated by RT-qPCR, where it was
301 shown to be a very early event in the course of reprogramming, with a greater than 50%
302 reduction of the control *Zfp36l1* mRNA levels only 24h after the first transfection (day2)
303 (**Suppl.Fig.4A**). Interestingly, ISX9 alone was not potent to down-regulate *Zfp36l1* mRNA levels

304 (**Fig.5C**), further supporting our initial hypothesis that ISX9 alone cannot instruct
305 reprogramming of astrocytes to iNs, possibly by failing to down-regulate astrocytic fate genes.

306 Since Zfp36l1 acts by mediating degradation of its mRNA targets, we were interested in
307 identifying Zfp36l1 mRNA targets, being up-regulated in our analysis. For this purpose, we
308 combined two publicly available Zfp36l1 individual-nucleotide resolution CLIP-Seq data (iCLIP-
309 Seq) from thymocytes (Vogel et al. 2016) and B lymphocytes (Galloway et al. 2016) and ended
310 up with 621 Zfp36l1 direct targets that are up-regulated in miR-124-iNs vs sc-miRNA astro
311 ($\log_2$(fold change)≥1, FDR<0.05), which importantly correspond to 47% of miR-124 up-
312 regulated DEGs. GO enrichment analysis revealed that many of these genes are implicated in
313 neurogenesis, neuron projection development, synaptic transmission, axonogenesis,
314 dendritic morphogenesis and telencephalon development (**Fig.5D**). Interestingly, many of
315 them were also found to regulate transcription and RNA processing (**Fig.5D**), highlighting an
316 important regulatory role for many Zfp36l1 targets, which could possibly have great impact
317 on the reprogramming process. Among these targets we found neurogenic TFs, such as *Tox,*
318 *Tox3, Rcor2, Cux1, Hes6, Lzts1* and *Mllt11* as well as EFs also related to neurogenesis such as
319 *Chd3, Chd7, Kmt2c* and *Tet1* (**Fig.5E**). Notably, we also identified as Zfp36l1 direct targets the
320 neuronal RBPs *Elavl4, Nova1* and *Rbfox1* (**Fig.5E**). This constitutes a significant finding that
321 delineates the neuronal RBPs' repression directly by Zfp36l1, being relieved upon miR-124-
322 mediated Zfp36l1 down-regulation.

323 We subsequently examined the mRNA levels of the Zfp36l1 targets, *Elavl*4, *Nova1, Rbfox1,*
324 *Rcor2* and *Tox* upon miR-124 overexpression with RT-qPCR and verified that miR-124 was
325 potent to induce their up-regulation (**Fig.5F**). We also verified the increase of the protein
326 levels of the neurogenic TF and target of Zfp36l1, Tox, in miR-124-iNs at day5 by
327 immunofluorescence analysis (**Suppl.Fig.4B, C**).

328 Notably, we observed that the combination of miR-124 with ISX9 greatly further enhanced
329 the mRNA levels of the RBP targets of Zfp36l1, *Elavl4* and *Rbfox1* (**Suppl.Fig.4D**), as well as the
330 other neuronal RBPs of the nElavl family, *Elavl2* (**Suppl.Fig.4E**) and *Elavl3* (**Suppl.Fig.4F**),
331 highlighting the importance of ISX9 in reinforcing the mRNA levels of significant neuronal
332 specific RBPs during the course of reprogramming.

333 Collectively, these data show that the targeting of Zfp36l1 by miR-124 de-represses the
334 Zfp36l1 neurogenic interactome, which corresponds to half of the miR-124-up-regulated
335 genes and includes neuronal-specific genes with important regulatory functions. Thus the

336 miR-124/Zfp36l1 interaction bears the potential to play a key regulatory role in the control of
337 the neurogenic reprogramming switch of astrocytes by miR-124.

338 **Targeting of Zfp36l1 by miR-124 plays a key role in the miR-124-induced cell fate switch of**
339 **astrocytes to iNs**

340 To investigate the impact of the miR-124/Zfp36l1 interaction on the miR-124-mediated
341 reprogramming of astrocytes, we used a target site blocker (TSB) oligonucleotide, which
342 competitively binds to the miR-124 binding site on the 3'UTR of Zfp36l1 mRNA and blocks its
343 down-regulation by the miR-124-RISC complex (**Fig.6A**). We verified the inhibition of the miR-
344 124-induced down-regulation of Zfp36l1 protein levels by the addition of TSB in a dose
345 dependent manner (miR-124:TSB molecular ratio 4:1, 2:1) at day5 of the reprogramming
346 protocol by western blot (**Fig.6B**). Next, we tested the effect of TSB on the mRNA levels of the
347 neuronal targets of Zfp36l1, *Tox, Rbfox1, Nova1, Rcor2* and *Elavl4* by RT-qPCR initially at day3
348 and observed a dose-dependent reduction of the miR-124-induced up-regulation of *Tox,*
349 *Rbfox1, Nova1* and *Rcor2*, but not of *Elavl4*, in the presence of increasing concentrations of
350 TSB (miR-124:TSB molecular ratio 4:1, 2:1 and 1:1) (**Fig.6C**). The mRNA levels of *Tox* and *Rbfox1*
351 retained the same response to TSB at a later time point, at day5 (**Suppl.Fig.5A, B**), an effect
352 that was not observed for the other Zfp36l1 targets *Nova1*, *Rcor2* and *Elavl4* (**Suppl.Fig.5C**),
353 implying that their post-transcriptional regulation becomes more complex as the neuronal
354 conversion is gradually established. Importantly, TSB resulted in a statistically significant and
355 dose-dependent reduction in the percentage of Tuj1+ miR-124-iNs at day5 (**Fig.6D, E**), which
356 was accompanied by an evident alteration of their characteristic iN morphology (**Fig.6D, F**).
357 More specifically, a morphological analysis of the number of processes extending from the
358 soma and the size of the soma of Tuj1+ cells indicated that TSB addition resulted in gradual
359 abolishment of their multipolar neuronal morphology with fine processes, characteristic of
360 miR-124-iNs (**Fig.6D left panel, F**), and instead largely led to the retention of a premature
361 astrocyte-like morphology with bigger soma (**Suppl.Fig.5D**) and none or very few processes
362 (**Fig.6D right panel, F**).

363 These observations strongly indicate that the targeting of Zfp36l1 by miR-124 plays a crucial
364 role in the miR-124-induced neuronal reprogramming action by unlocking neurogenic genes
365 with important regulatory activity and by controlling the necessary morphological changes.

366

367

368 **miR-124 induces reprogramming of resident reactive astrocytes to iNs with deep-layer**
369 **cortical identity *in vivo* following cortical trauma**

370 To evaluate the *in vivo* reprogramming potential of miR-124 to drive cell fate conversion of
371 resident reactive cortical astrocytes to iNs alone or supplemented by ISX9, we overexpressed
372 miR-124 via lentiviral transfer into the mechanically injured cortex of 3-4 months old mice. To
373 this end we stereotaxically injected either one of the two lentiviruses, control LV-GFP and LV-
374 miR-124-GFP, in order to transduce reactive astrocytes surrounding the cortical injury site,
375 whileISX9 was systemically administered beginning 2 days afterviral injection for 5
376 consecutive days in a group of mice (**Fig.7A**). We initially sacrificed a group of mice 6 days after
377 viral administration (10 days after cortical trauma induction) to evaluate the original
378 phenotype of transduced cells surrounding the injury site (**Suppl.Fig.6A**) and observed that
379 the majority of them (approximately 68%)in both conditions were GFAP+ reactive astrocytes,
380 while an average of 10% were NeuN+ neurons. The rest of the transduced cells were equally
381 either Iba-1+ microglial cells or Olig2+oligodendrocytes (**Suppl.Fig.6B**). For all markers
382 examined at this time point, there were no statistically significant differences between LV-
383 124-GFP and control LV-GFP, indicating that the two viruses are expected to transduce the
384 same percentage of astrocytes and neurons upon injection into the cortical parenchyma.
385 Further analysis of the percentage of NeuN+/GFP+ transduced cells 3 weeks after the
386 stereotaxic injection revealed that it was significantly increased in the animals that received
387 the miR-124-overexpressing virus, but not the control virus (**Fig.7B, C**). In particular, while
388 approximately 10% of the transduced cells were NeuN+ in LV-GFP-injected animals, showing
389 no significant difference between the 6 days and 3 week time points, 74% of the LV-miR-124-
390 GFP-transduced cells were NeuN+ 3 weeks after the injection, showing significant difference
391 between the two time points, indicating a strong potential of miR-124 to direct conversion of
392 reactive astrocytes into iNs *in vivo*. The same effect was observed when the injection of LV-
393 miR-124-GFPvirus was accompanied by systemic administration of ISX9, where 71% of
394 transduced cells were found to be NeuN+, while no significant difference was observed at 3
395 weeks after co-treatment of ISX9 in comparison to LV-miR-124-GFP injection alone (**Fig.7C**).

396 Overexpression of miR-124either alone or along with ISX9 administration, appeared to drive
397 iNs towards a deep layer cortical identity, as the vast majority of the NeuN+ transduced cells
398 after 3 weeks in both groups were also positive for the deep layer cortical marker Tbr1, with
399 percentages reaching 98% in LV-miR-124-iNs and 88% in LV-miR-124-GFP+ISX9-iNs, with no
400 significant difference observed between the two groups (**Fig.7D, E**).

401 The above *in vivo* data indicate that miR-124 is sufficient to drive on its own neurogenic
402 reprogramming of reactive astrocytes within the injured cortex micro-environment that
403 render it a potent candidate molecule for further in vivo application.

404

405 ## Discussion

406 In this study we attempted to isolate miR-124 mechanism of action from that of other
407 reprogramming co-factors and we provide evidence that miR-124 drives the trans-
408 differentiation switch of cortical astrocytes to an immature iN phenotype of cortical identity,
409 recapitulating its endogenous role in embryonic cortical development (Maiorano and
410 Mallamaci 2009) and SVZ adult neurogenesis (Cheng et al. 2009; Åkerblom et al. 2012).
411 Indeed, miR-124 directed astrocytes through a multipolar intermediate stage expressing TFs
412 such as *Mash1, Tbr2, Insm1, Rcor2, Fezf2* and *Tbr1* all associated with neuronal commitment
413 and differentiation during embryonic (Kwan, Šestan, and Anton 2012; Elsen et al. 2018)and
414 adult neurogenesis (Díaz-Guerra et al. 2013). Intriguingly, miR-124 over-expression led to a
415 significant down-regulation of the neuronal differentiation bHLH TF NeuroD1, which has been
416 reported as a temporal, stage-specific event in early stages of eye development in Xenopus
417 (Liu et al. 2011). To this end to reinforce the differentiation of immature miR-124-iNs, we
418 supplemented miR-124 with the neurogenic compound ISX9, known to up-regulate neuronal
419 specific genes, among which NeuroD1. ISX9 acts by increasing intracellular Ca^{2+} signaling
420 leading to HDAC5 nuclear exit and MEF2 de-repression (Schneider et al. 2008) and has been
421 already used in chemical reprogramming protocols for the conversion of fibroblasts and
422 astrocytes to iNs (Gao et al. 2017; Xiang Li et al. 2015). Additionally, ISX9 enhances the
423 differentiation of iPSC-derived neurons from Huntington's disease patients, indicating that it
424 also possesses a neuronal maturation-promoting activity (Lim et al. 2017). Indeed, the
425 addition of ISX9 greatly improved both the reprogramming efficiency and differentiation
426 status of miR-124+ISX9-iNs, by enhancing *Tbr2, Neurog2* and *NeuroD1* transcriptional levels
427 reinforcing their passage through a Tbr2+ intermediate stage and subsequently promoting
428 their differentiation leading to the acquisition of electrophysiologically active iNs.
429 Interestingly, despite a robust up-regulation of the levels of NeuroD1 and many other
430 neuronal TFs by ISX9 alone, control sc-miRNA+ISX9-treated astrocytes failed to undergo
431 reprogramming. NeuroD1 has been extensively reported to possess a strong 'pioneer factor'
432 reprogramming capacity towards the neuronal fate upon its viral-mediated overexpression
433 (Pataskar et al. 2016; Matsuda et al. 2019; Guo et al. 2014; Rivetti Di Val Cervo et al. 2017),
434 however we hypothesize that very high levels of *NeuroD1* – not being triggered by ISX9
435 supplementation in our system – are required to inflict these effects.

436 The RNA-Seq analysis we performed, highlighted the importance of miR-124 over-expression
437 in the down-regulation of astrocytic TFs, RBPs, EFs and components of signaling pathways with
438 significant regulatory role in astrocytic identity and function, which is in accordance with the

439 documented role of miR-124 in favoring neuronal fate at the expense of astrocytic (Neo et al.
440 2014) and implies that astrocytic identity barriers need to be repressed before the induction
441 of a neuronal cell fate during the reprogramming process. Conversely, ISX9 had a small
442 contribution in the repression of astrocytic genes, thus this might be the reason for its inability
443 to confer the reprogramming switch on its own.

444 Our analysis of the direct miR-124 targets utilizing AGO-HITS-CLIP data from mouse cortex (Chi
445 et al. 2009) revealed the RBP *Zfp36l1* as a novel target of miR-124. Of note, we also verified
446 the miR-124/Zfp36l1 interaction in human bearing the same binding site, by analyzing AGO-
447 HITS-CLIP data from human motor cortex and cingulate gyrus (Boudreau et al. 2014), a finding
448 highlighting the importance of this conserved interaction during mammalian brain evolution.
449 Many studies have identified several direct targets of miR-124 with important regulatory role
450 in neurogenesis, acting at the transcriptional level, such as the TFs *Sox9* (Cheng et al. 2009),
451 Lhx2 (Sanuki et al. 2011) and the components of the REST repressor complex, *Scp1*
452 (Visvanathan et al. 2007) and *Rcor1* (Baudet et al. 2012; Volvert et al. 2014); or at the
453 epigenetic level, such as the component of the PRC2 complex *Ezh2* (Neo et al. 2014) and the
454 component of the BAF complex BAF53a (Yoo et al. 2009); as well as at the post-transcriptional
455 level, such as the RBP involved in alternative splicing Ptbp1 (Makeyev et al. 2007).

456 Here, we report for the first time that miR-124 is directly implicated in the regulation of
457 another process mediated by RBPs, the mRNA decay, apart from the well-characterized miR-
458 124/Ptbp1 circuitry (Makeyev et al. 2007; Yeom et al. 2018; Xue et al. 2013). Zfp36l1 is a
459 member of the Zfp36 family of proteins along with Zfp36 and Zfp36l2, which act by binding to
460 AU rich elements (AREs) in the 3'UTR of their mRNA targets mediating their destabilization(Lai
461 et al. 2000). Zfp36l1 is expressed in cortical radial glial precursors of the VZ (Yuzwa et al. 2017;
462 Weng et al. 2019; DeBoer et al. 2013), in cortical glial cells (Weng et al. 2019) and in non-
463 neuronal cells (Carrick and Blackshear 2007; Chen et al. 2015). Interestingly, the ARE-
464 dependent mRNA decay is regulated by other neurogenic miRNAs as well, since the close
465 paralog of Zfp36l1, Zfp36, is targeted by miR-9 (Dai et al. 2015), suggesting a combined
466 regulation of Zfp36 family members by the two miRNAs to counteract the destabilization of
467 neuronal mRNAs during neurogenesis.

468 In order to identify targets of Zfp36l1 being up-regulated in our system we examined data
469 from Zfp36l1-iCLIP-Seq experiments in thymocytes (Vogel et al. 2016) and B lymphocytes
470 (Galloway et al. 2016). Although our analysis was restricted to a not relevant to the astrocytic
471 transcriptome, we identified a rather large number of Zfp36l1 targets being up-regulated in
472 miR-124-iNs that interestingly correspond to nearly half of the up-regulated genes by miR-

473 124. Importantly, many Zfp36l1 targets exhibit significant regulatory role in neurogenesis and
474 neuronal differentiation, such as the studied here TFs *Tox* and *Rcor2* and the RBPs *Rbfox1*,
475 *Elavl4,* and *Nova1*. Further on, to experimentally validate our hypothesis that Zfp36l1 is a
476 direct miR-124 target implicated in astrocytes' cell fate switch, we used a target site blocker
477 (TSB) that efficiently antagonizes the binding of miR-124 in the 3'UTR of *Zfp36l1* mRNA and
478 showed that the disruption of miR-124/Zfp36l1 interaction has a negative impact on the
479 reprogramming process, reducing the number of Tuj1+ miR-124-iNs and abolishing their
480 multipolar morphology. Of note, our experiments with the TSB blocker revealed that among
481 the neuron-specific RBPs that are targets of Zfp36l1, *Rbfox1* and *Nova1* exhibit a pattern of
482 direct post-transcriptional regulation by contrast to *Elavl4*, implying the stronger involvement
483 of other RBPs in its post-transcriptional regulation. In accordance with this, Zfp36 has been
484 reported to target *Elavl2, Elavl3, Elavl4* and *Nova1* (Dai et al. 2015), uncovering a
485 complementary and synergistic role of Zfp36l1 and Zfp36 in repressing neuron-specific RBPs
486 in non-neuronal cells.

487 Importantly, the here identified Zfp36l1 direct target, *Rbfox1*, has been reported to be a
488 critical post-transcriptional regulator of gene expression during cortical development (J. A. Lee
489 et al. 2016; Weyn-Vanhentenryck et al. 2014). To the same direction, we show here that
490 Zfp36l1 also directly targets the TFs *Tox* and *Rcor2*, both known to be involved in the control
491 of mammalian corticogenesis, with Tox regulating among others the levels of dorsal
492 telenchephalon TFs and marker of IPs Tbr2 (Artegiani et al. 2015) and Rcor2 being expressed
493 along with Insm1 in cortical IPs promoting dorsal telencephalon patterning (Wang et al. 2016;
494 Elsen et al. 2018). Additionally, the repression of the multipolar morphology of miR-124-iNs
495 by the TSB blocker could imply a role for the miR-124/Zfp36l1 interaction in the acquisition of
496 a multipolar morphology characteristic of endogenous VZ/SVZ IPs (Mizutani et al.,2018), a fact
497 corroborated by the GO analysis of Zfp36l1 target genes, which presented the GO terms
498 neuronal projection development and dendrite morphogenesis with high statistical
499 significance. Thus, this analysis revealed certain transcriptional and post-transcriptional
500 cortical neurogenesis regulators being de-repressed by the miR124/Zfp36l1 interaction
501 **(Fig.6G)**, strengthening the notion that miR-124-mediated reprogramming of astrocytes
502 recapitulates molecular aspects of endogenous neurogenesis.

503 Furthermore, the addition of ISX9 significantly contributed to the up-regulation of the mRNA
504 levels of the neuronal RBPs *Elavl2, Elavl3, Elavl4* (Ince-Dunn et al. 2012; Scheckel et al. 2016)
505 and *Rbfox1* (Weyn-Vanhentenryck et al. 2014), reinforcing the action of miR-124 in inducing
506 the switch from the neuronal transcripts' destabilizing RBPs to the stabilizing neuronal RBPs

507 (**Fig.6G**). In parallel, ISX9 supplementation greatly enhanced the transcriptional levels and the
508 number of TFs related to telencephalon development and/or adult neurogenesis, further
509 promoting the cortical identity of iNs already initiated by miR-124. Surprisingly, ISX9 also up-
510 regulated a large set of TFs related to the development of other non-telencephalic brain
511 regions such as the midbrain and the hindbrain/spinal cord. However, the mechanism of the
512 observed here ISX9-mediated up-regulation of ventral/caudal TFs still remains elusive. Of
513 note, ISX9 has been shown to affect the epigenetic landscape leading to an open chromatin
514 state by increasing H3/H4 acetylation in pancreatic β-cells (Dioum et al. 2011), suggesting that
515 an epigenetic mechanism may be responsible for the observed transcriptional regional
516 expansion, a hypothesis that needs to be further explored.

517 Here we also demonstrate that miR-124 is capable of directly converting reactive cortical
518 astrocytes surrounding a mechanically-induced trauma to iNs of deep-layer cortical identity.
519 Brain injury is known to facilitate in vivo reprogramming, rendering astrocytes more plastic by
520 activating NSC genes' expression (Götz et al. 2015). *In vivo* reprogramming of reactive
521 astrocytes to neuronal precursors and iNs has been achieved following forced expression of
522 TFs among which Sox2 (Niu et al. 2013), Neurog2 (Grande et al. 2013), NeuroD1 (Guo et al.
523 2014; Rivetti Di Val Cervo et al. 2017) and Nurr1/Neurog2 (Mattugini et al. 2019), in some
524 cases combined with anti-apoptotic and/or anti-oxidant treatment to enhance survival
525 (Gascón et al. 2016). However, it is the first time that miR-124 is shown to be sufficient to
526 reprogram reactive astrocytes to NeuN+ iNs with a high efficiency of 74%. Unlike to the *in*
527 *vitro* situation, co-administration of ISX9 didn't significantly further enhance miR-124-induced
528 reprogramming efficiency *in vivo*, possibly reflecting the strong effect of the surrounding
529 micro-environment in supporting miR-124-induced neuronal conversion. Indeed, pro-
530 inflammatory cytokines like TNF, and growth factors such as EGF, FGF2 and SHH present in
531 the injured cortex have been reported to facilitate the neurogenic conversion of astrocytes
532 (Gabel et al. 2016; Grande et al. 2013; Sirko et al. 2013).

533 Interestingly, following either miR-124 or miR-124+ISX9 treatment all iNs possess a deep-layer
534 cortical identity expressing Tbr1 protein. Taking into account the fact that the injury has been
535 performed in a deep cortical area, this observation indicates that, besides the *in vitro* observed
536 endogenous potency of reprogrammed iNs to up-regulate Tbr1 levels, region-specific
537 neuronal identity barriers are imposed to newly produced iNs by the surrounding cortical
538 microenvironment, in accordance with recent findings unravelling the existence of layer-
539 driven neuronal identity during *in vivo* astrocytic reprogramming to iNs (Mattugini et al. 2019).

540 Taken together this study highlighted the strong potency of miR-124 to instruct the cell fate
541 switch of astrocytes, post-transcriptionally triggering cortical neurogenesis pathways being
542 unlocked by the direct targeting of *Zfp36l1*. Additionally, our *in vitro* results give mechanistic
543 insight from a developmental perspective into the combined action of miR-124 and ISX9 in
544 driving direct reprogramming of astrocytes to mature iNs. Importantly, our findings point to
545 an even stronger *in vivo* reprogramming capacity of miR-124 than the one observed *in vitro*,
546 opening the possibility for its use in therapeutic protocols with minimal support by other
547 neurogenic or anti-inflammatory/anti-oxidant factors.

548

549 # Materials and Methods

550 **Primary cultures of postnatal cortical astrocytes**

551 Primary postnatal astrocytic cultures from P3-P5 mice were prepared as previously described
552 (Aravantinou-Fatorou et al. 2015). Briefly, the cerebral cortexes from 2-3 P3-P5 C57BL/6 mice
553 were collected in ice cold HBSS (Invitrogen), the tissue was washed three times with HBSS and
554 digested with 0.04% trypsin (Sigma) and 10μg/ml DNAse (Sigma) for 5 min at 37°C. After
555 digestion cells were mechanically dissociated, centrifuged for 5 min at 850 rpm (120 g), re-
556 suspended in DMEM 4.5g/lt glucose (Invitrogen) containing 10% FBS (Invitrogen), 1%
557 Penicillin/Streptomycin (Pen/Strep) (Sigma) and placed in a T75 flask pre-coated with poly-D-
558 lysine (PDL) (Sigma). When culture reached confluence (usually after 7 days), the flask was
559 shaken in a horizontal shaker at 200-250 rpm for 20h, in order to obtain a pure astrocytic
560 culture, free from neurons, oligodendrocytes and microglia. The remaining cells were digested
561 with 0.5% trypsin-EDTA (Invitrogen) for 5 min at 37°C, centrifuged at 850 rpm, re-suspended
562 in fresh DMEM 4.5g/lt glucose 10% FBS, 1% Pen/Strep and divided in two new T75 flasks pre-
563 coated with PDL. Half of the medium was changed every two days.

564 **In vitro reprogramming protocol**

565 For the reprogramming of astrocytes to induced-neurons, 40,000 astrocytes were seeded in
566 10mm coverslips coated with 20μg/ml poly-L-ornithine (PLO) (Sigma) overnight and 5μg/ml
567 laminin for 3 h at 37°C (Sigma). Once cells reached>90% confluence (usually after 1-2 days)
568 they became transfected with 80nM miR-124-3p mimics or sc-miRNA mimics (negative
569 control) (Thermo) using Lipofectamine 2000 (Invitrogen) according to manufacturer's
570 instructions (day1). The next day the astrocytic medium (DMEM 4.5g/lt glucose, 10% FBS, 1%
571 Pen/Strep) was replaced with the reprogramming medium: Neurobasal (Invitrogen)
572 supplemented with 1X B-27 (Invitrogen), 1X GlutaMAX (Invitrogen), 20μM vitamin E (a-
573 tocopherol) (Sigma) and 200mM ascorbic acid (Sigma). The same process of transfection was
574 repeated twice at day3 and day5. Vitamin E was added to the medium until day4, while
575 ascorbic acid was added throughout the reprogramming protocol. At day7 the reprogramming
576 medium was changed to the neuronal differentiation medium: Neurobasal supplemented
577 with 1X B-27, 1X GlutaMAX, 20ng/ml BDNF (R&D Systems), 0.5mM cAMP (Sigma) and 200mM
578 ascorbic acid. In the miR-124+ISX9-reprogrammed cells, 10μM of ISX9 chemical compound
579 (Tocris) were added from day2 to day10. All the mediums added to the reprogrammed cells
580 were pre-conditioned for 24 h in a confluent astrocytic culture.

581

582 **RT-qPCR analysis**

583 For the RT-qPCR analysis experiments, total RNA was extracted using the Nucleospin miRNA
584 kit (Macherey-Nagel) and 500-800ng of total RNA were used for cDNA synthesis with the
585 Superscript II reverse transcriptase (Invitrogen) according to manufacturer's instructions.
586 Quantitative real time PCR was performed using SYBR Select Master Mix (Applied Biosystems)
587 and samples were run in the ViiA 7 Real-Time PCR System (Applied Biosystems). The primers
588 used are listed in **Table 1**. Each sample was analyzed in triplicates, gene expression was
589 calculated using the ΔΔCt method and all the results were normalized to β-actin expression.
590 Relative expression was estimated setting the values of sc-miRNA transfected astrocytes to 1.
591 All experiments were performed at least in triplicates.

592 **Immunocytochemistry**

593 Cells were washed once with PBS and then fixed with 4% paraformaldehyde for 20 min at
594 room temperature. Afterwards, cells were washed three times with PBS and blocked with 5%
595 normal donkey serum (NDS) (Merck-Millipore), 0.1% Triton X-100 in PBS for 1 h at room
596 temperature. For nuclear staining, cells were permeabilized with 0.25% Triton X-100 in PBS
597 for 10 min at room temperature and washed three times with PBS prior to blocking. Next, cells
598 were incubated with primary antibodies, diluted in 1% NDS, 0.05% Triton X-100 in PBS
599 overnight at 4°C. The next day, cells were washed three times with PBS and incubated with
600 secondary antibodies diluted in 1% NDS, 0.05% Triton X-100 in PBS for 2h at room
601 temperature. The nuclei of the cells were stained with ProLong Gold Antifade Reagent with
602 DAPI (Cell Signalling). The following primary antibodies were used in this study: mouse anti-
603 Tuj1 (Covance, 1:600), chicken anti-Tuj1 (Millipore, 1:1000), mouse anti-MAP2 (Millipore,
604 1:200), rabbit anti-Synapsin1 (Abcam, 1:200), rat anti-Mash1 (R&D Systems, 1:100), rabbit
605 anti-Tbr2 (Abcam, 1:200), rabbit anti-Gsx2 (Millipore, 1:400), rabbit anti-Tox (Atlas antibodies,
606 1:200), mouse anti-vGlut1 (Millipore, 1:1000) and rabbit anti-GABA (Sigma, 1:10,000). The
607 secondary antibodies used in this study were Alexa Fluor 546-, Alexa Fluor 488- and Alexa
608 Fluor 647-conjugated secondary antibodies (Life Technologies). Images were acquired with a
609 20x or 40x objective (1024x1024 pixels, 1µm Z-step) using a Leica TCS SP8 confocal microscope
610 (LEICA Microsystems). For each experiment measurements from 20-25 fields per coverslip
611 were obtained for each condition.

612

613

614 **Electrophysiology**

615 For whole-cell recordings iNs plated in PLO-laminin coated coverslips were used for
616 electrophysiological experiments beginning at day15 up to day27 of the reprogramming
617 protocol. The coverslips with the cells were placed onto a recording chamber and viewed using
618 an Olympus CKX41 microscope with a 40x lens. The cells were bathed in a solution containing:
619 140mM NaCl, 2.8mM KCl, 2mM $CaCl_2$, 4mM $MgCl_2$, 10mM Glucose, and 20mM HEPES. For
620 whole-cell recordings we used a capillary glass with Filament (Sutter instrument) to fabricate
621 low resistance recording pipettes (~5 MΩ) and filled with: 140mM KCl, 2mM $CaCl_2$, 2mM
622 $MgCl_2$, 2mM Mg-ATP, 5mM EGTA and 10mM HEPES. Osmolarity and pH of all solutions were
623 adjusted appropriately before experiments. Data were acquired at room temperature (22–
624 24°C) using an EPC9 HEKA amplifier and an ITC-16 acquisition system with a patchmaster
625 software (HEKA). Data analysis was carried out using OriginPro8. **Voltage protocols:** The
626 membrane of the cells was held at a holding potential of -70 mV and step depolarizing pulses
627 were applied. Depolarization steps were applied for 50 msec in 10 mV increments from -80
628 mV to +50 mV with a sweep interval time of 1 sec and sweep duration of 500 ms. Each
629 depolarizing pulse was proceeded by a hyperpolarizing step to -120 mV. **Current protocols:**
630 Cells we held at their resting membrane potential (0pA) and depolarizing current steps from -
631 20 pA to 200 pA from a holding current of 0pA were applied.

632 **RNA-Seq experiment and bioinformatic analysis**

633 For the RNA-Seq experiment, the following samples were prepared in 3 biological replicates:
634 astrocytes (day1), sc-miRNA-transfected astrocytes (day7), miR-124-iNs (day7) and miR-
635 124+ISX9-iNs (day7). Total RNA was extracted using the Nucleospin miRNA kit (Macherey-
636 Nagel) according to manufacturer's instructions. Libraries were prepared with TruSeq RNA
637 Library Prep Kit v2 (Illumina) and 75c single-end sequencing in an Illumina NextSeq 550
638 sequencer. Raw libraries were quality checked and preprocessed using FastQC
639 (https://www.bioinformatics.babraham.ac.uk/projects/fastqc/). Mapping of reads against
640 the Mouse Transcriptome (v.GRCm38.rel79) and transcript abundance estimation on
641 Transcripts Per Million (TPM) values was performed using kallisto (Bray et al. 2016). Analysis
642 of differential expression, interpretation and visualization was subsequently performed using
643 kallisto-compatible Sleuth tool (Pimentel et al. 2017) and R-base functions. Gene ontology
644 (GO) enrichment analysis was performed using the Gene Ontology Panther Classification
645 System (http://pantherdb.org/).

646

647 **Analysis of AGO-CLIP-Seq data**

648 AGO-HITS-CLIP datasets, performed in mouse brain cortex tissue (P13 neocortex, 5 replicates)
649 and human brain tissues (motor cortex, cingulate gyrus) from 2 individuals, were retrieved
650 from the publications (Chi et al. 2009) and (Boudreau et al. 2014) respectively. Raw libraries
651 were quality checked using FastQC (www.bioinformatics.babraham.ac.uk/projects/fastqc/),
652 while adapters/ contaminants were detected utilizing an in-house developed pipeline and the
653 Kraken suite (Davis et al. 2013). Pre-processing was performed with TrimGalore (Krueger
654 2015) and Cutadapt (Martin 2011). CLIP-Seq libraries were aligned against the reference
655 genomes, i.e. GRCh38 and mm10 assemblies for human and mouse respectively, with
656 GMAP/GSNAP (Wu and Nacu 2010) spliced aligner, allowing up to 2 mismatches. microCLIP
657 CLIP-Seq-guided model (Paraskevopoulou et al. 2018) was utilized to identify binding events
658 for the expressed miRNAs. In case of multiple replicates (i.e. mouse brain cortex) a miRNA
659 binding event had to be present in at least two replicates to be considered as valid. Top
660 expressed miRNAs were retrieved from the relevant publications. Human and mouse
661 transcriptomes were compiled from ENSEMBL v96 (Cunningham et al. 2019) to annotate the
662 retrieved miRNA binding events. Identified miRNA binding sites residing on 3' UTR regions
663 were retained and subsequently filtered to preserve only genes expressed in astrocytes. A list
664 of ~10,000 genes, expressed in astrocytes, with FPKM ≥ 2, was retrieved from a reference
665 publication and retained for analysis (Y. Zhang et al. 2014).

666 **Target Site Blocker (TSB) experiment**

667 For the functional validation of the miR-124/Zfp36l1 interaction a custom made miRCURY
668 locked nucleic acid (LNA) miRNA Power Target Site Blocker (TSB) (Qiagen) was used with the
669 following sequence: TTACAAGGCACTAAGTTGCTT. TSB was transfected in astrocytes along
670 with sc-miRNA or miR-124-3p mimics using Lipofectamine 2000 (Invitrogen) in different
671 molecular ratios: miR-124:TSB, 4:1 (80nM:20nM), 2:1 (80nM:40nM) and 1:1 (80nM:80nM).

672 **Western blot**

673 Cells were washed once with ice-cold PBS and lysed for 15 min in ice-cold lysis buffer (150mM
674 NaCl, 50mM Tris (pH 7.5), 1%v/v Triton X-100, 1mM EDTA, 1mM EGTA, 0.1% SDS, 0.5% sodium
675 deoxycholate) containing PhosSTOP phosphatase inhibitors and a complete protease inhibitor
676 mixture (Roche Life Science), then centrifuged at 20,000 g for 15 min, followed by collection
677 of the supernatant and measurement of the protein concentration by Bradford assay
678 (Applichem). Proteins were separated by SDS-polyacrylamide gel electrophoresis (PAGE) and
679 transferred onto nitrocellulose membranes (Maine Manufacturing). Nonspecific binding sites

680 were blocked in TBS/ 0.1% Tween 20/5% skimmed milk for 1 hour at 20°C followed by
681 overnight incubation with primary antibodies diluted in TBS/0.1% Tween20/5% BSA. Primary
682 antibodies used were rabbit anti-Zfp36l1 (Abcam, 1:500) and mouse anti-βactin (Millipore,
683 1:1000). Incubation with HRP-conjugated secondary antibodies, anti-mouse-HRP (Thermo,
684 1:10,000) and anti-rabbit-HRP (Thermo, 1:5,000) was performed for 2 hours at room
685 temperature and protein bands were visualized using the Clarity Western ECL Substrate (BIO-
686 RAD).

687 **Lentiviral production**

688 For lentiviral in vivo transduction, VSV-G (Vesicular Stomatitis Virus–Glycoprotein)–
689 pseudotyped lentiviruses were used either for the over-expression of miR-124 along with GFP
690 or as control expressing only GFP. More specifically, for lentiviral particles' production, HEK
691 293T cells cultured in 10-cm Petri dishes at a 50-60% confluence were co-transfected with 10
692 µg lentiviral plasmid expressing miR-124-1 precursor under the CMV promoter and GFP under
693 the EF1 promoter (SBI System Biosciences) or 10 µg lentiviral plasmid expressing GFP under
694 the CMV promoter and the packaging plasmids pVSV-G (3.5 µg), MDL (6.5 µg), and RSV-REV
695 (2.5 µg) (all kindly provided by Dr. Matsas lab) with calcium phosphate. The following day the
696 culture medium was replaced with fresh one, the supernatant containing the lentiviral
697 particles was collected 48 h and 72 h (second harvest) after transfection and concentrated by
698 ultracentrifugation at 25,000 rpm (80,000 x g) for 2 h at 4°C using a sucrose gradient.

699 **Cortical trauma, viral injection and ISX9 administration**

700 This study was carried out in strict compliance with the European Directive 2010/63/EU and
701 the Greek National Law 161/91 for Use of Laboratory Animals, according to FELASA
702 recommendations for euthanasia and the National Institutes of Health Guide for Care and Use
703 of Laboratory Animals. All protocols were approved by the Animal Care and Use Committee
704 of the Hellenic Pasteur Institute (Animal House Establishment Code: EL 25 BIO 013). License
705 No 2585/29-5-18 for the experiments was issued by the Greek authorities of the Veterinary
706 Department of the Athens Prefecture. The manuscript was prepared in compliance with the
707 ARRIVE guidelines for reporting animal research.
708 Adult male and female FVB mice (8-16 weeks old) were deeply anaesthetized using inhalable
709 isoflurane, and positioned in a stereotaxic apparatus. The dorsal surface of the skull was
710 exposed through a midline incision and a burr hole was drilled at the following coordinates:
711 antero-posterior (AP) -1.0 mm, caudal to Bregma; lateral (L) 1.0 mm to the midline (Franklin
712 and Paxinos, 2001). A 26-gauge needle was inserted into the brain parenchyma in a depth of
713 0.9 mm from the surface of the brain to create a trauma in the cortex, avoiding the corpus

714 callosum and hippocampus. The inserted needle was moved along the anterior-posterior axis
715 between positions (AP) -1.1 and -0.9 to widen the trauma. The skin was sutured, a local
716 analgesic cream containing 2.5% lidocain and 2.5% prilocain was applied and the animals were
717 kept warm until they were fully awake. Viral injection took place 4 days after the cortical
718 trauma. A 10µl Hamilton syringe (Hamilton) with a 26-gauge needle was slowly inserted into
719 the brain tissue at coordinates (AP) -1.1 mm, (L) 1.0 mm, and (V): 1.0 mm, from the same burr
720 hole on the skull and 2µl of lentiviral concentrate was injected at a rate of 0.5 µl/min. The
721 needle was left in position for 5 min after each injection and then withdrawn gently. A second
722 viral injection was repeated at coordinates (AP) -0.9 mm, (L) 1.0 mm, and (V): 1.0 mm with
723 similar procedures, and surgery was completed as described above. A group of animals was
724 injected with the lentivirus LV-miR-124-GFP (group LV-124) and another one with the control
725 lentivirus LV-GFP (group LV-GFP). A subgroup of the LV-124 group received intraperitoneally
726 20 mg/kg of ISX9 (Tocris) diluted in (2-Hydroxypropyl)-β-cyclodextrin (Sigma) (ISX9
727 concentration: 2 mg/ml in 30% (2-Hydroxypropyl)-β-cyclodextrin (Sigma) diluted in sterile
728 ddH2O) once a day, for 5 consecutive days, beginning 48 h after lentiviral injection. Animals
729 were sacrificed 6 days or 3 weeks after viral injection.

730 **Tissue Preparation, Histology, and Immunohistochemistry**

731 For histology, mice were deeply anaesthetized by inhaling isoflurane, and perfused with 4%
732 paraformaldehyde (PFA) via left cardiac ventricle. The brains were removed, post-fixed in 4%
733 PFA overnight, and then cryo-protected in 20% sucrose overnight. Tissues were then frozen
734 in -20°C isopentane and cut into 20 µm-thick coronal sections on a cryostat (Leica CM1900),
735 collected on silane-coated slides and stored at -20°C. For detection of specific antigens with
736 immunofluorescence, sections were left for 15 min in room temperature, washed in PBS, and
737 blocked with 5% normal goat or donkey serum (Merck-Millipore) in PBT (0.1% Triton X-
738 100/PBS) for 1 h. Incubation with primary antibodies took place overnight at 4°C. Primary
739 antibodies to assess transduced cell identity used were: chicken polyclonal anti-GFP (Abcam,
740 1:1000) to detect the transplanted cells, mouse monoclonal anti-neuronal nuclei (NeuN)
741 (Merck-Millipore, 1:300) to identify mature neurons, rabbit polyclonal anti-glial fibrillary acidic
742 protein (GFAP) (Dako,1:600) to detect astrocytes; rabbit polyclonal anti-oligodendrocyte
743 transcription factor 2 (Olig2) (Merck-Millipore, 1:200) to detect oligodendrodytes, rabbit
744 polyclonal anti-ionized calcium-binding adapter 1 (Iba-1) (Wako, 1:600) for detection of
745 microglia and rabbit polyclonal anti-Tbr1 (Abcam,1:250) for detection of deep layer cortical
746 neurons. Following incubation with primary antibodies, sections were washed with PBS and
747 incubated for 2 h with the appropriate secondary antibodies conjugated with AlexaFluor 488

748 (green), 546 (red), or 647 (blue) and Hoechst (Molecular Probes) for nuclei staining. Finally,
749 sections were washed and coverslipped with Mowiol (Calbiochem). Images were acquired
750 with a 40x objective using Leica TCS SP8 and Leica TCS-SP5II confocal microscopes (LEICA
751 Microsystems).

752 **Image analysis**

753 Images were analyzed using Fiji/ImageJ software (National Institutes of Health).
754 **In vitro analysis:** mean fluorescence intensity of Tbr2, Tox and Mash1 staining inside the cell
755 nuclei was quantified using a custom-written macro implemented in Fiji. Initially automatic
756 detection of nuclei was performed using the Otsu method and Tuj1+ cells were selected
757 based on their mean intensity value above a user-defined threshold of 40, followed by a
758 manual validation according to cell morphology (cells with an astrocyte-like morphology with
759 a big, rectangular soma and none or few processes were excluded). Mean fluorescence
760 intensity of Tbr2, Tox and Mash1 inside the cell nuclei ROIs was measured both for Tuj1- and
761 Tuj1+ cells. Quantification was performed in maximum intensity projections. For each
762 experiment measurements from at least 200-300 cells were obtained for each condition.
763 Morphological characterization of Tuj1+ cells in the TSB blocker experiments was also
764 conducted using Fiji. More specifically, morphological characterization included quantification
765 of the cell body area and the number of processes extending from the soma of Tuj1+ cells.
766 Tuj1+ cells were selected based on the mean intensity value of their soma above a user-
767 defined threshold and were sorted in 3 groups: cells with a multipolar morphology bearing 3
768 or more processes extending from the soma, cells with 1-2 processes and cells exhibiting an
769 astrocyte-like morphology with a rectangular soma possessing none or 1-2 processes.
770 Quantification was performed in maximum intensity projections. For each experiment
771 measurements from at least 100-150 cells were obtained for each condition.
772 **In vivo analysis:** for each animal and each immunofluorescence staining, cell counting was
773 performed on brain sections collected at 240 lm intervals across the whole antero-posterior
774 extent of the hippocampus (bregma-0.5mm up to -2.5mm) in a total number of 3-4 mice for
775 each experimental condition. For estimation of the ratio of transduced cells that have a
776 specific phenotype, images of all GFP+ cells found in each set of sections were acquired and
777 double-positivity with cell type-specific markers was evaluated by an observer "blind" to
778 treatment group and time point. All GFP+ cells found in the cortex within these sections were
779 imaged and analyzed. Representative confocal images shown in **Fig.7** and **Suppl.Fig.6** are
780 obtained from coronal sections, antero-posterior positions between 21.3 and 22.2 relative to
781 Bregma.

782 **Statistical analysis**

783 All in vitro quantified data are presented as average ± SD, unless otherwise indicated. Two-
784 tailed Student t-test was used to calculate statistical significance with p values for all the data
785 obtained from the experiments with the TSB blocker, while for the rest of the data a one-
786 tailed Student t-test was used. p values less than 0.05 ($p<0.05$) were considered indicative of
787 significance. In vivo data were assessed using a one-way analysis of variance (ANOVA). When
788 interactions were detected, group comparisons were performed using a two-sample assuming
789 unequal variances test.

790 **Data Availability**

791 High throughput sequencing data are deposited in the European Nucleotide Archive under
792 Study accession PRJEB38603.

793

Acknowledgments

This work was financially supported by: 'BIOIMAGING-GR: A Greek Research Infrastructure for Visualizing and Monitoring Fundamental Biological Processes (MIS 5002755)', funded by the Operational Program "Competitiveness, Entrepreneurship and Innovation" (NSRF 2014-2020), co-financed by Greece and the European Union (European Regional Development Fund); ARISTEIA-II 'Astro-Rep' 3713 Excellence Grant of the Greek Ministry of Education and Fondation Santé Grant 2017-2018, awarded to DT. We also acknowledge funding from the Stavros Niarhos Foundation (SFN) Grant to the Hellenic Pasteur Institute, as part of the Foundation's initiative to support the Greek Research Center ecosystem; Greek General Secretariat of Research and Technology 'Action for the Study of Neurodegenerative Diseases on the Basis of Precision Medicine' and 'KRIPIS-II' Action (MIS 5002486) under the Operational Strategic Reference Framework 2014–2020. We would like to thank Dr. Era Taoufik for critical comments on the manuscript.

Author Contributions

EP and DT conceived whole project, designed experiments and analyzed the data; EP, CG and MM conducted in vitro experiments; DCT and SJT designed and performed electrophysiology experiments; TK, DK and AGH designed and performed bioinformatics analysis and EP contributed in analyzing the data; PNK designed and performed in vivo experiments, analyzed relevant data and contributed in paper writing; IT contributed to in vivo experiments and relevant data analysis; EX developed the Fiji macro and helped with image analysis workflow; EP and DT wrote the manuscript; DT supervised the project and acquired funding.

Conflict of Interest

The authors report no conflict of interest.

818 # References

819 Abernathy, Daniel G., Woo Kyung Kim, Matthew J. McCoy, Allison M. Lake, Rebecca Ouwenga, Seong
820 Won Lee, Xiaoyun Xing, et al. 2017. "MicroRNAs Induce a Permissive Chromatin Environment
821 That Enables Neuronal Subtype-Specific Reprogramming of Adult Human Fibroblasts." *Cell Stem*
822 *Cell* 21 (3): 332-348.e9. https://doi.org/10.1016/j.stem.2017.08.002.
823 Acaz-Fonseca, Estefania, Ana Ortiz-Rodriguez, Iñigo Azcoitia, Luis M. Garcia-Segura, and Maria
824 Angeles Arevalo. 2019. "Notch Signaling in Astrocytes Mediates Their Morphological Response
825 to an Inflammatory Challenge." *Cell Death Discovery*. https://doi.org/10.1038/s41420-019-
826 0166-6.
827 Åkerblom, Malin, Rohit Sachdeva, Isabelle Barde, Sonia Verp, Bernhard Gentner, Didier Trono, and
828 Johan Jakobsson. 2012. "MicroRNA-124 Is a Subventricular Zone Neuronal Fate Determinant."
829 *Journal of Neuroscience*. https://doi.org/10.1523/JNEUROSCI.0558-12.2012.
830 Ambasudhan, Rajesh, Maria Talantova, Ronald Coleman, Xu Yuan, Saiyong Zhu, Stuart A. Lipton, and
831 Sheng Ding. 2011. "Direct Reprogramming of Adult Human Fibroblasts to Functional Neurons
832 under Defined Conditions." *Cell Stem Cell*. https://doi.org/10.1016/j.stem.2011.07.002.
833 Aravantinou-Fatorou, Katerina, Felipe Ortega, Dafni Chroni-Tzartou, Nasia Antoniou, Cornelia
834 Poulopoulou, Panagiotis K. Politis, Benedikt Berninger, Rebecca Matsas, and Dimitra
835 Thomaidou. 2015. "CEND1 and NEUROGENIN2 Reprogram Mouse Astrocytes and Embryonic
836 Fibroblasts to Induced Neural Precursors and Differentiated Neurons." *Stem Cell Reports* 5 (3):
837 405–18. https://doi.org/10.1016/j.stemcr.2015.07.012.
838 Artegiani, Benedetta, Antonio M Jesus Domingues, Sara Bragado Alonso, Elisabeth Brandl, Simone
839 Massalini, Andreas Dahl, and Federico Calegari. 2015. "Tox: A Multifunctional Transcription
840 Factor and Novel Regulator of Mammalian Corticogenesis." *The EMBO Journal* 34 (7): 896–910.
841 https://doi.org/10.15252/embj.201490061.
842 Baudet, Marie Laure, Krishna H. Zivraj, Cei Abreu-Goodger, Alistair Muldal, Javier Armisen, Cherie
843 Blenkiron, Leonard D. Goldstein, Eric A. Miska, and Christine E. Holt. 2012. "MiR-124 Acts
844 through CoREST to Control Onset of Sema3A Sensitivity in Navigating Retinal Growth Cones."
845 *Nature Neuroscience*. https://doi.org/10.1038/nn.2979.
846 Berninger, Benedikt, Marcos R. Costa, Ursula Koch, Timm Schroeder, Bernd Sutor, Benedikt Grothe,
847 and Magdalena Götz. 2007. "Functional Properties of Neurons Derived from in Vitro
848 Reprogrammed Postnatal Astroglia." *Journal of Neuroscience*.
849 https://doi.org/10.1523/JNEUROSCI.1615-07.2007.
850 Birtele, Marcella, Yogita Sharma, Srisaiyini Kidnapillai, Shong Lau, Thomas B. Stoker, Roger A. Barker,
851 Daniella Rylander Ottosson, Janelle Drouin-Ouellet, and Malin Parmar. 2019. "Dual Modulation
852 of Neuron-Specific MicroRNAs and the REST Complex Promotes Functional Maturation of
853 Human Adult Induced Neurons." *FEBS Letters*. https://doi.org/10.1002/1873-3468.13612.
854 Boudreau, Ryan L., Peng Jiang, Brian L. Gilmore, Ryan M. Spengler, Rebecca Tirabassi, Jay A. Nelson,
855 Christopher A. Ross, Yi Xing, and Beverly L. Davidson. 2014. "Transcriptome-Wide Discovery of
856 MicroRNA Binding Sites in Human Brain." *Neuron*.
857 https://doi.org/10.1016/j.neuron.2013.10.062.
858 Bray, Nicolas L., Harold Pimentel, Páll Melsted, and Lior Pachter. 2016. "Near-Optimal Probabilistic
859 RNA-Seq Quantification." *Nature Biotechnology*. https://doi.org/10.1038/nbt.3519.
860 Carrick, Danielle M., and Perry J. Blackshear. 2007. "Comparative Expression of Tristetraprolin (TTP)
861 Family Member Transcripts in Normal Human Tissues and Cancer Cell Lines." *Archives of*
862 *Biochemistry and Biophysics*. https://doi.org/10.1016/j.abb.2007.04.011.
863 Chen, Ming Tai, Lei Dong, Xin Hua Zhang, Xiao Lin Yin, Hong Mei Ning, Chao Shen, Rui Su, et al. 2015.
864 "ZFP36L1 Promotes Monocyte/Macrophage Differentiation by Repressing CDK6." *Scientific*
865 *Reports*. https://doi.org/10.1038/srep16229.
866 Cheng, Li Chun, Erika Pastrana, Masoud Tavazoie, and Fiona Doetsch. 2009. "MiR-124 Regulates Adult
867 Neurogenesis in the Subventricular Zone Stem Cell Niche." *Nature Neuroscience*.
868 https://doi.org/10.1038/nn.2294.
869 Chi, Sung Wook, Julie B. Zang, Aldo Mele, and Robert B. Darnell. 2009. "Argonaute HITS-CLIP Decodes
870 MicroRNA-MRNA Interaction Maps." *Nature*. https://doi.org/10.1038/nature08170.
871 Cunningham, Fiona, Premanand Achuthan, Wasiu Akanni, James Allen, M. Ridwan Amode, Irina M.
872 Armean, Ruth Bennett, et al. 2019. "Ensembl 2019." *Nucleic Acids Research*.

https://doi.org/10.1093/nar/gky1113.
Dai, Weijun, Wencheng Li, Mainul Hoque, Zhuyun Li, Bin Tian, and Eugene V. Makeyev. 2015. "A Post-Transcriptional Mechanism Pacing Expression of Neural Genes with Precursor Cell Differentiation Status." *Nature Communications*. https://doi.org/10.1038/ncomms8576.
Davis, Matthew P.A., Stijn van Dongen, Cei Abreu-Goodger, Nenad Bartonicek, and Anton J. Enright. 2013. "Kraken: A Set of Tools for Quality Control and Analysis of High-Throughput Sequence Data." *Methods*. https://doi.org/10.1016/j.ymeth.2013.06.027.
DeBoer, E. M., M. L. Kraushar, R. P. Hart, and M. R. Rasin. 2013. "Post-Transcriptional Regulatory Elements and Spatiotemporal Specification of Neocortical Stem Cells and Projection Neurons." *Neuroscience*. https://doi.org/10.1016/j.neuroscience.2013.05.042.
Deo, Monika, Jenn Yah Yu, Kwan Ho Chung, Melissa Tippens, and David L. Turner. 2006. "Detection of Mammalian MicroRNA Expression by in Situ Hybridization with RNA Oligonucleotides." *Developmental Dynamics*. https://doi.org/10.1002/dvdy.20847.
Díaz-Guerra, Eva, Jaime Pignatelli, Vanesa Nieto-Estévez, and Carlos Vicario-Abejón. 2013. "Transcriptional Regulation of Olfactory Bulb Neurogenesis." *Anatomical Record*. https://doi.org/10.1002/ar.22733.
Dioum, Elhadji M., Jihan K. Osborne, Sean Goetsch, Jamie Russell, Jay W. Schneider, and Melanie H. Cobb. 2011. "A Small Molecule Differentiation Inducer Increases Insulin Production by Pancreatic β Cells." *Proceedings of the National Academy of Sciences of the United States of America*. https://doi.org/10.1073/pnas.1118526109.
Elsen, Gina E., Francesco Bedogni, Rebecca D. Hodge, Theo K. Bammler, James W. MacDonald, Susan Lindtner, John L.R. Rubenstein, and Robert F. Hevner. 2018. "The Epigenetic Factor Landscape of Developing Neocortex Is Regulated by Transcription Factors Pax6→ Tbr2→ Tbr1." *Frontiers in Neuroscience*. https://doi.org/10.3389/fnins.2018.00571.
Gabel, Sebastien, Eric Koncina, Gauthier Dorban, Tony Heurtaux, Cindy Birck, Enrico Glaab, Alessandro Michelucci, Paul Heuschling, and Luc Grandbarbe. 2016. "Inflammation Promotes a Conversion of Astrocytes into Neural Progenitor Cells via NF-KB Activation." *Molecular Neurobiology*. https://doi.org/10.1007/s12035-015-9428-3.
Galloway, Alison, Alexander Saveliev, Sebastian Łukasiak, Daniel J. Hodson, Daniel Bolland, Kathryn Balmanno, Helena Ahlfors, et al. 2016. "RNA-Binding Proteins ZFP36L1 and ZFP36L2 Promote Cell Quiescence." *Science*. https://doi.org/10.1126/science.aad5978.
Gao, Longfei, Wuqiang Guan, Min Wang, Huihan Wang, Jiali Yu, Qing Liu, Binlong Qiu, et al. 2017. "Direct Generation of Human Neuronal Cells from Adult Astrocytes by Small Molecules." *Stem Cell Reports*. https://doi.org/10.1016/j.stemcr.2017.01.014.
Gascón, Sergio, Elisa Murenu, Giacomo Masserdotti, Felipe Ortega, Gianluca L. Russo, David Petrik, Aditi Deshpande, et al. 2016. "Identification and Successful Negotiation of a Metabolic Checkpoint in Direct Neuronal Reprogramming." *Cell Stem Cell* 18 (3): 396–409. https://doi.org/10.1016/j.stem.2015.12.003.
Götz, Magdalena, Swetlana Sirko, Johannes Beckers, and Martin Irmler. 2015. "Reactive Astrocytes as Neural Stem or Progenitor Cells: In Vivo Lineage, In Vitro Potential, and Genome-Wide Expression Analysis." *GLIA*. https://doi.org/10.1002/glia.22850.
Grande, Andrew, Kyoko Sumiyoshi, Alejandro López-Juárez, Jennifer Howard, Bhuvaneswari Sakthivel, Bruce Aronow, Kenneth Campbell, and Masato Nakafuku. 2013. "Environmental Impact on Direct Neuronal Reprogramming in Vivo in the Adult Brain." *Nature Communications* 4. https://doi.org/10.1038/ncomms3373.
Gross, Robert E., Mark F. Mehler, Peter C. Mabie, Ziying Zang, Linda Santschi, and John A. Kessler. 1996. "Bone Morphogenetic Proteins Promote Astroglial Lineage Commitment by Mammalian Subventricular Zone Progenitor Cells." *Neuron*. https://doi.org/10.1016/S0896-6273(00)80193-2.
Guo, Ziyuan, Lei Zhang, Zheng Wu, Yuchen Chen, Fan Wang, and Gong Chen. 2014. "In Vivo Direct Reprogramming of Reactive Glial Cells into Functional Neurons after Brain Injury and in an Alzheimer's Disease Model." *Cell Stem Cell* 14 (2): 188–202. https://doi.org/10.1016/j.stem.2013.12.001.
Heinrich, Christophe, Robert Blum, Sergio Gascón, Giacomo Masserdotti, Pratibha Tripathi, Rodrigo Sánchez, Steffen Tiedt, Timm Schroeder, Magdalena Götz, and Benedikt Berninger. 2010. "Directing Astroglia from the Cerebral Cortex into Subtype Specific Functional Neurons." *PLoS Biology*. https://doi.org/10.1371/journal.pbio.1000373.

930 Ince-Dunn, Gulayse, Hirotaka J. Okano, Kirk B. Jensen, Woong Yang Park, Ru Zhong, Jernej Ule, Aldo
931 Mele, et al. 2012. "Neuronal Elav-like (Hu) Proteins Regulate RNA Splicing and Abundance to
932 Control Glutamate Levels and Neuronal Excitability." *Neuron*.
933 https://doi.org/10.1016/j.neuron.2012.07.009.
934 Jiang, Houbo, Zhimin Xu, Ping Zhong, Yong Ren, Gaoyang Liang, Haley A. Schilling, Zihua Hu, et al.
935 2015. "Cell Cycle and P53 Gate the Direct Conversion of Human Fibroblasts to Dopaminergic
936 Neurons." *Nature Communications*. https://doi.org/10.1038/ncomms10100.
937 Kang, Wenfei, and Jean M. Hébert. 2011. "Signaling Pathways in Reactive Astrocytes, a Genetic
938 Perspective." *Molecular Neurobiology*. https://doi.org/10.1007/s12035-011-8163-7.
939 Krueger, Felix. 2015. "Trim Galore!: A Wrapper Tool around Cutadapt and FastQC to Consistently
940 Apply Quality and Adapter Trimming to FastQ Files." *Babraham Institute*.
941 Kwan, Kenneth Y., Nenad Šestan, and E. S. Anton. 2012. "Transcriptional Co-Regulation of Neuronal
942 Migration and Laminar Identity in the Neocortex." *Development*.
943 https://doi.org/10.1242/dev.069963.
944 Lai, Wi S., Ester Carballo, Judith M. Thorn, Elizabeth A. Kennington, and Perry J. Blackshear. 2000.
945 "Interactions of CCCH Zinc Finger Proteins with MRNA. Binding of Tristetraprolin-Related Zinc
946 Finger Proteins to AU-Rich Elements and Destabilization of MRNA." *Journal of Biological*
947 *Chemistry*. https://doi.org/10.1074/jbc.M001696200.
948 Lee, Ji Ann, Andrey Damianov, Chia Ho Lin, Mariana Fontes, Neelroop N. Parikshak, Erik S. Anderson,
949 Daniel H. Geschwind, Douglas L. Black, and Kelsey C. Martin. 2016. "Cytoplasmic Rbfox1
950 Regulates the Expression of Synaptic and Autism-Related Genes." *Neuron*.
951 https://doi.org/10.1016/j.neuron.2015.11.025.
952 Lee, Seong Won, Young Mi Oh, Ya Lin Lu, Woo Kyung Kim, and Andrew S. Yoo. 2018. "MicroRNAs
953 Overcome Cell Fate Barrier by Reducing EZH2-Controlled REST Stability during Neuronal
954 Conversion of Human Adult Fibroblasts." *Developmental Cell*.
955 https://doi.org/10.1016/j.devcel.2018.06.007.
956 Li, Xiang, Xiaohan Zuo, Junzhan Jing, Yantao Ma, Jinlin Jiaming Wang, Defang Liu, Jialiang Zhu, et al.
957 2015. "Small-Molecule-Driven Direct Reprogramming of Mouse Fibroblasts into Functional
958 Neurons." *Cell Stem Cell* 17 (2): 195–203. https://doi.org/10.1016/j.stem.2015.06.003.
959 Li, Xuekun, and Peng Jin. 2010. "Roles of Small Regulatory RNAs in Determining Neuronal Identity."
960 *Nature Reviews Neuroscience*. https://doi.org/10.1038/nrn2739.
961 Lim, Ryan G., Lisa L. Salazar, Daniel K. Wilton, Alvin R. King, Jennifer T. Stocksdale, Delaram Sharifabad,
962 Alice L. Lau, et al. 2017. "Developmental Alterations in Huntington's Disease Neural Cells and
963 Pharmacological Rescue in Cells and Mice." *Nature Neuroscience* 20 (5): 648–60.
964 https://doi.org/10.1038/nn.4532.
965 Liu, Kaili, Ying Liu, Weichuan Mo, Rong Qiu, Xiumei Wang, Jane Y. Wu, and Rongqiao He. 2011. "MiR-
966 124 Regulates Early Neurogenesis in the Optic Vesicle and Forebrain, Targeting NeuroD1."
967 *Nucleic Acids Research*. https://doi.org/10.1093/nar/gkq904.
968 Luján, R., R. Shigemoto, and G. López-Bendito. 2005. "Glutamate and GABA Receptor Signalling in the
969 Developing Brain." *Neuroscience*. https://doi.org/10.1016/j.neuroscience.2004.09.042.
970 Magnusson, Jens P., Christian Göritz, Jemal Tatarishvili, David O. Dias, Emma M.K. Smith, Olle Lindvall,
971 Zaal Kokaia, and Jonas Frisén. 2014. "A Latent Neurogenic Program in Astrocytes Regulated by
972 Notch Signaling in the Mouse." *Science*. https://doi.org/10.1126/science.346.6206.237.
973 Maiorano, Nicola Antonio, and Antonello Mallamaci. 2009. "Promotion of Embryonic Cortico-Cerebral
974 Neuronogenesis by MiR-124." *Neural Development*. https://doi.org/10.1186/1749-8104-4-40.
975 Makeyev, Eugene V., Jiangwen Zhang, Monica A. Carrasco, and Tom Maniatis. 2007. "The MicroRNA
976 MiR-124 Promotes Neuronal Differentiation by Triggering Brain-Specific Alternative Pre-MRNA
977 Splicing." *Molecular Cell*. https://doi.org/10.1016/j.molcel.2007.07.015.
978 Martin, Marcel. 2011. "Cutadapt Removes Adapter Sequences from High-Throughput Sequencing
979 Reads." *EMBnet.Journal*. https://doi.org/10.14806/ej.17.1.200.
980 Matsuda, Taito, Takashi Irie, Shutaro Katsurabayashi, Yoshinori Hayashi, Tatsuya Nagai, Nobuhiko
981 Hamazaki, Aliya Mari D. Adefuin, et al. 2019. "Pioneer Factor NeuroD1 Rearranges
982 Transcriptional and Epigenetic Profiles to Execute Microglia-Neuron Conversion." *Neuron*.
983 https://doi.org/10.1016/j.neuron.2018.12.010.
984 Mattugini, Nicola, Riccardo Bocchi, Volker Scheuss, Gianluca Luigi Russo, Olof Torper, Chu Lan Lao,
985 and Magdalena Götz. 2019. "Inducing Different Neuronal Subtypes from Astrocytes in the
986 Injured Mouse Cerebral Cortex." *Neuron* 103 (6): 1086-1095.e5.

987 https://doi.org/10.1016/j.neuron.2019.08.009.
988 Mizutani, Ken Ichi. 2018. "Physiological Significance of Multipolar Cells Generated from Neural Stem
989 Cells and Progenitors for the Establishment of Neocortical Cytoarchitecture." *Genes to Cells*.
990 https://doi.org/10.1111/gtc.12546.
991 Neo, Wen Hao, Karen Yap, Suet Hoay Lee, Liang Sheng Looi, Piyush Khandelia, Sheng Xiong Neo,
992 Eugene V. Makeyev, and I. Hsin Su. 2014. "MicroRNA MiR-124 Controls the Choice between
993 Neuronal and Astrocyte Differentiation by Fine-Tuning Ezh2 Expression." *Journal of Biological*
994 *Chemistry*. https://doi.org/10.1074/jbc.M113.525493.
995 Niu, Wenze, Tong Zang, Yuhua Zou, Sanhua Fang, Derek K. Smith, Robert Bachoo, and Chun Li Zhang.
996 2013. "In Vivo Reprogramming of Astrocytes to Neuroblasts in the Adult Brain." *Nature Cell*
997 *Biology* 15 (10): 1164–75. https://doi.org/10.1038/ncb2843.
998 Paraskevopoulou, Maria D., Dimitra Karagkouni, Ioannis S. Vlachos, Spyros Tastsoglou, and Artemis G.
999 Hatzigeorgiou. 2018. "MicroCLIP Super Learning Framework Uncovers Functional
1000 Transcriptome-Wide MiRNA Interactions." *Nature Communications*.
1001 https://doi.org/10.1038/s41467-018-06046-y.
1002 Pataskar, Abhijeet, Johannes Jung, Pawel Smialowski, Florian Noack, Federico Calegari, Tobias Straub,
1003 and Vijay K Tiwari. 2016. "NeuroD1 Reprograms Chromatin and Transcription Factor Landscapes
1004 to Induce the Neuronal Program." *The EMBO Journal*.
1005 https://doi.org/10.15252/embj.201591206.
1006 Pimentel, Harold, Nicolas L. Bray, Suzette Puente, Páll Melsted, and Lior Pachter. 2017. "Differential
1007 Analysis of RNA-Seq Incorporating Quantification Uncertainty." *Nature Methods*.
1008 https://doi.org/10.1038/nmeth.4324.
1009 Rivetti Di Val Cervo, Pia, Roman A. Romanov, Giada Spigolon, Débora Masini, Elisa Martín-Montañez,
1010 Enrique M. Toledo, Gioele La Manno, et al. 2017. "Induction of Functional Dopamine Neurons
1011 from Human Astrocytes in Vitro and Mouse Astrocytes in a Parkinson's Disease Model." *Nature*
1012 *Biotechnology*. https://doi.org/10.1038/nbt.3835.
1013 Sanuki, Rikako, Akishi Onishi, Chieko Koike, Rieko Muramatsu, Satoshi Watanabe, Yuki Muranishi,
1014 Shoichi Irie, et al. 2011. "MiR-124a Is Required for Hippocampal Axogenesis and Retinal Cone
1015 Survival through Lhx2 Suppression." *Nature Neuroscience*. https://doi.org/10.1038/nn.2897.
1016 Scheckel, Claudia, Elodie Drapeau, Maria A. Frias, Christopher Y. Park, John Fak, Ilana Zucker-Scharff,
1017 Yan Kou, et al. 2016. "Regulatory Consequences of Neuronal ELAV-like Protein Binding to Coding
1018 and Non-Coding RNAs in Human Brain." *ELife*. https://doi.org/10.7554/eLife.10421.
1019 Schneider, Jay W., Zhengliang Gao, Shijie Li, Midhat Farooqi, Tie Shan Tang, Ilya Bezprozvanny, Doug
1020 E. Frantz, and Jenny Hsieh. 2008. "Small-Molecule Activation of Neuronal Cell Fate." *Nature*
1021 *Chemical Biology* 4 (7): 408–10. https://doi.org/10.1038/nchembio.95.
1022 Sirko, Swetlana, Gwendolyn Behrendt, Pia Annette Johansson, Pratibha Tripathi, Marcos Costa, Sarah
1023 Bek, Christophe Heinrich, et al. 2013. "Reactive Glia in the Injured Brain Acquire Stem Cell
1024 Properties in Response to Sonic Hedgehog Glia." *Cell Stem Cell*.
1025 https://doi.org/10.1016/j.stem.2013.01.019.
1026 Torper, Olof, Ulrich Pfisterer, Daniel A. Wolf, Maria Pereira, Shong Lau, Johan Jakobsson, Anders
1027 Björklund, Shane Grealish, and Malin Parmar. 2013. "Generation of Induced Neurons via Direct
1028 Conversion in Vivo." *Proceedings of the National Academy of Sciences of the United States of*
1029 *America* 110 (17): 7038–43. https://doi.org/10.1073/pnas.1303829110.
1030 Victor, Matheus B., Michelle Richner, Tracey O. Hermanstyne, Joseph L. Ransdell, Courtney Sobieski,
1031 Pan Yue Deng, Vitaly A. Klyachko, Jeanne M. Nerbonne, and Andrew S. Yoo. 2014. "Generation
1032 of Human Striatal Neurons by MicroRNA-Dependent Direct Conversion of Fibroblasts." *Neuron*.
1033 https://doi.org/10.1016/j.neuron.2014.10.016.
1034 Victor, Matheus B., Michelle Richner, Hannah E. Olsen, Seong Won Lee, Alejandro M. Monteys,
1035 Chunyu Ma, Christine J. Huh, et al. 2018. "Striatal Neurons Directly Converted from
1036 Huntington's Disease Patient Fibroblasts Recapitulate Age-Associated Disease Phenotypes."
1037 *Nature Neuroscience*. https://doi.org/10.1038/s41593-018-0075-7.
1038 Visvanathan, Jaya, Soo Kyung Seunghee Lee, Bora Lee, Jae W. Lee, and Soo Kyung Seunghee Lee.
1039 2007. "The MicroRNA MiR-124 Antagonizes the Anti-Neural REST/SCP1 Pathway during
1040 Embryonic CNS Development." *Genes and Development*. https://doi.org/10.1101/gad.1519107.
1041 Vogel, Katharina U., Lewis S. Bell, Alison Galloway, Helena Ahlfors, and Martin Turner. 2016. "The
1042 RNA-Binding Proteins Zfp36l1 and Zfp36l2 Enforce the Thymic β-Selection Checkpoint by
1043 Limiting DNA Damage Response Signaling and Cell Cycle Progression." *The Journal of*

1044 *Immunology*. https://doi.org/10.4049/jimmunol.1600854.
1045 Volvert, Marie Laure, Pierre Paul Prévot, Pierre Close, Sophie Laguesse, Sophie Pirotte, James
1046 Hemphill, Florence Rogister, et al. 2014. "MicroRNA Targeting of CoREST Controls Polarization
1047 of Migrating Cortical Neurons." *Cell Reports*. https://doi.org/10.1016/j.celrep.2014.03.075.
1048 Wang, Yixuan, Qian Wu, Peng Yang, Chenfei Wang, Jing Liu, Wenyu Ding, Wensu Liu, et al. 2016.
1049 "LSD1 Co-Repressor Rcor2 Orchestrates Neurogenesis in the Developing Mouse Brain." *Nature*
1050 *Communications*. https://doi.org/10.1038/ncomms10481.
1051 Weng, Qinjie, Jincheng Wang, Jiajia Wang, Danyang He, Zuolin Cheng, Feng Zhang, Ravinder Verma, et
1052 al. 2019. "Single-Cell Transcriptomics Uncovers Glial Progenitor Diversity and Cell Fate
1053 Determinants during Development and Gliomagenesis." *Cell Stem Cell*.
1054 https://doi.org/10.1016/j.stem.2019.03.006.
1055 Weyn-Vanhentenryck, Sebastien M., Aldo Mele, Qinghong Yan, Shuying Sun, Natalie Farny, Zuo
1056 Zhang, Chenghai Xue, et al. 2014. "HITS-CLIP and Integrative Modeling Define the Rbfox
1057 Splicing-Regulatory Network Linked to Brain Development and Autism." *Cell Reports*.
1058 https://doi.org/10.1016/j.celrep.2014.02.005.
1059 Wohl, Stefanie Gabriele, and Thomas Andrew Reh. 2016. "MiR-124-9-9* Potentiates Ascl1-Induced
1060 Reprogramming of Cultured Müller Glia." *GLIA*. https://doi.org/10.1002/glia.22958.
1061 Wu, Thomas D., and Serban Nacu. 2010. "Fast and SNP-Tolerant Detection of Complex Variants and
1062 Splicing in Short Reads." *Bioinformatics*. https://doi.org/10.1093/bioinformatics/btq057.
1063 Xue, Yuanchao, Kunfu Ouyang, Jie Huang, Yu Zhou, Hong Ouyang, Hairi Li, Gang Wang, et al. 2013.
1064 "Direct Conversion of Fibroblasts to Neurons by Reprogramming PTB-Regulated MicroRNA
1065 Circuits." *Cell* 152 (1–2): 82–96. https://doi.org/10.1016/j.cell.2012.11.045.
1066 Yang, Chunzhang, Rajiv R. Iyer, Albert C.H. Yu, Raymund L. Yong, Deric M. Park, Robert J. Weil, Barbara
1067 Ikejiri, Roscoe O. Brady, Russell R. Lonser, and Zhengping Zhuang. 2012. "β-Catenin Signaling
1068 Initiates the Activation of Astrocytes and Its Dysregulation Contributes to the Pathogenesis of
1069 Astrocytomas." *Proceedings of the National Academy of Sciences of the United States of*
1070 *America*. https://doi.org/10.1073/pnas.1118754109.
1071 Yeom, Kyu Hyeon, Simon Mitchell, Anthony J. Linares, Sika Zheng, Chia Ho Lin, Xiao Jun Wang,
1072 Alexander Hoffmann, and Douglas L. Black. 2018. "Polypyrimidine Tract-Binding Protein Blocks
1073 MiRNA-124 Biogenesis to Enforce Its Neuronal-Specific Expression in the Mouse." *Proceedings*
1074 *of the National Academy of Sciences of the United States of America*.
1075 https://doi.org/10.1073/pnas.1809609115.
1076 Yoo, Andrew S., Brett T. Staahl, Lei Chen, and Gerald R. Crabtree. 2009. "MicroRNA-Mediated
1077 Switching of Chromatin-Remodelling Complexes in Neural Development." *Nature*.
1078 https://doi.org/10.1038/nature08139.
1079 Yoo, Andrew S., Alfred X. Sun, Li Li, Aleksandr Shcheglovitov, Thomas Portmann, Yulong Li, Chris Lee-
1080 Messer, Ricardo E. Dolmetsch, Richard W. Tsien, and Gerald R. Crabtree. 2011. "MicroRNA-
1081 Mediated Conversion of Human Fibroblasts to Neurons." *Nature*.
1082 https://doi.org/10.1038/nature10323.
1083 Yuzwa, Scott A., Michael J. Borrett, Brendan T. Innes, Anastassia Voronova, Troy Ketela, David R.
1084 Kaplan, Gary D. Bader, and Freda D. Miller. 2017. "Developmental Emergence of Adult Neural
1085 Stem Cells as Revealed by Single-Cell Transcriptional Profiling." *Cell Reports*.
1086 https://doi.org/10.1016/j.celrep.2017.12.017.
1087 Zhang, Lei, Jiu Chao Yin, Hana Yeh, Ning Xin Ma, Grace Lee, Xiangyun Amy Chen, Yanming Wang, et al.
1088 2015. "Small Molecules Efficiently Reprogram Human Astroglial Cells into Functional Neurons."
1089 *Cell Stem Cell*. https://doi.org/10.1016/j.stem.2015.09.012.
1090 Zhang, Ye, Kenian Chen, Steven A. Sloan, Mariko L. Bennett, Anja R. Scholze, Sean O'Keeffe, Hemali P.
1091 Phatnani, et al. 2014. "An RNA-Sequencing Transcriptome and Splicing Database of Glia,
1092 Neurons, and Vascular Cells of the Cerebral Cortex." *Journal of Neuroscience*.
1093 https://doi.org/10.1523/JNEUROSCI.1860-14.2014.
1094

1095

1096 # Figure legends

1097 **Figure 1: miR-124 is sufficient to instruct reprogramming of postnatal cortical astrocytes to**
1098 **iNs**

1099 **(A)** Overview of the miR-124-mediated reprogramming protocol. **(B)** Immunostaining of
1100 astrocytes reprogrammed with miR-124 at day7 and day14 of the reprogramming protocol
1101 with anti-Tuj1 antibody. **(C)** Quantification of the percentage of Tuj1+ reprogrammed cells
1102 (average ± SD, n=4 independent experiments, **p<0.01 and ***p<0.001 versus sc-miRNA).
1103 RT-qPCR analysis of the mRNA levels of the proneural TFs, *Mash1* and *Neurog2* **(D)**, the dorsal
1104 telencephalon TFs, *Tbr2, Tbr1, Fezf2, Cux1* **(E)**, the ventral telencephalon *TFs, Gsx2* and *Dlx1*
1105 **(F),** and the neuronal differentiation TFs, *Sox4, Sox11, Hes6* and *NeuroD1* **(G)**. Data are
1106 presented as fold change versus sc-miRNA (average ± SD, n=3 independent experiments,
1107 **p<0.01 and ***p<0.001 versus sc-miRNA). **(H)** Co-immunostaining of astrocytes
1108 reprogrammed with miR-124 at day7 of the reprogramming protocol with anti-Mash1/Tuj1,
1109 anti-Tbr2/Tuj1 and anti-Gsx2/Tuj1 antibodies. **(I)** Quantification of the percentage of Mash1+,
1110 Tbr2+ and Gsx2+ in Tuj1+ reprogrammed cells (average ± SD, n=3 independent experiments,
1111 **p<0.01 and ***p<0.001 versus sc-miRNA).

1112 **Figure 2: The neurogenic compound ISX9 greatly enhances the miR-124-induced**
1113 **reprogramming efficiency and differentiation state of iNs**

1114 **(A)** Immunostaining of astrocytes reprogrammed with miR-124 or miR-124+ISX9 at day7 and
1115 day14 of the reprogramming protocol with anti-Tuj1 antibody. **(B)** Quantification of the
1116 percentage of Tuj1+ reprogrammed cells at the timepoints day1, day5, day7, day10 and day14
1117 of the reprogramming protocol (average ± SD, n=3 independent experiments for day5 and
1118 day10, n=8 for day7 and n=4 for day14, *p<0.05 and ***p<0.001 versus miR-124). **(C)**RT-qPCR
1119 analysis of the mRNA levels of NeuroD1 at day7 of the reprogramming protocol. Data are
1120 presented as log_2(fold change) versus sc-miRNA (average ± SD, n=3 independent experiments,
1121 **p<0.01 and ***p<0.001 versus sc-miRNA). RT-qPCR analysis of the mRNA levels of the TFs,
1122 Neurog2 and Tbr2 (**D**) and Mash1 (**E**) at the time points day1, day5, day7, day10 and day14 of
1123 the reprogramming protocol. Data are presented as log_2(fold change) (**D**) and fold change (**E**)
1124 versus astrocytes (day1) (average ± SD, n=3 independent experiments, *p<0.05, **p<0.01 and
1125 ***p<0.001 versus miR-124). **(F)** Co-immunostaining of astrocytes reprogrammed with miR-
1126 124+ISX9 at day7 of the reprogramming protocol with anti-Mash1/Tuj1, anti-Tbr2/Tuj1 and
1127 anti-Gsx2/Tuj1 antibodies. **(G)** Quantification of the percentage of Mash1+, Tbr2+ and Gsx2+
1128 in Tuj1+ reprogrammed cells either with miR-124 or miR-124+ISX9 at day7 (average ± SD, n=3

1129 independent experiments, **p<0.01 versus miR-124). Measurement of the mean nuclear
1130 fluorescence intensity of Tbr2 **(H)** and Mash1 **(I)** in Tuj1+ reprogrammed cells either with miR-
1131 124 or miR-124+ISX9 at day7 (co-immunostaining with anti-Tbr2/Mash1/Tuj1 antibodies). A
1132 representative experiment is shown of n=3 independent experiments (mean ± SD, n=326 cells
1133 for miR-124 and n=540 cells for miR-124+ISX9, ***p<0.001 versus miR-124).

1134 **Figure 3: miR-124+ISX9-iNs exhibit characteristics of mature, electrophysiologically active**
1135 **neurons**

1136 **(A)** Co-immunostaining of miR-124+ISX9-iNs at day21 of the reprogramming protocol with
1137 anti-MAP2/Tuj1 and anti-MAP2/Synapsin1antibodies. Inset area indicated in white frame. **(B)**
1138 Quantification of the percentage of Tuj1+ miR-124-iNs and miR-124+ISX9-iNs at day21 of the
1139 reprogramming protocol. The percentage of MAP2/Syn1 double positive (DP) Tuj1+ iNs is
1140 shown in blue (average ± SD, n=3 independent experiments, ***p<0.001 refers to
1141 %MAP2/Syn1 DP in Tuj1+ miR-124+ISX9-iNs versus miR-124-iNs and ###p<0.001 refers to
1142 %Tuj1 miR-124+ISX9-iNs versus miR-124-iNs). **(C)** Co-immunostaining of miR-124+ISX9-iNs at
1143 day28 of the reprogramming protocol with anti-vGlut1/Tuj1 antibodies. **(D)** Quantification of
1144 the percentage of vGlut1+/Tuj1+ and GABA+/Tuj1+ miR-124+ISX9-iNs at day28 (average ± SD,
1145 n=3 independent experiments). **(E)** Superimposed traces of inward Na^+ currents and outward
1146 K^+ currents evoked by depolarizing voltage steps obtained from a miR-124+ISX9-iN (day22)
1147 (left panel). Superimposed traces of inward and outward currents evoked by the same
1148 protocol after 1 min pre-application of 1µM TTX + 10mM TEA, showing the inhibition of both
1149 inward and outward currents (middle panel), followed by full recovery of the current traces
1150 after 3 min wash of the cell (right panel). **(F)** Superimposed traces of inward Na^+ currents and
1151 outward K^+ currents evoked by depolarizing voltage steps obtained from a miR-124+ISX9-iN
1152 (day27). **(G)** Example of a repetitive action potential induced from a mature miR-124+ISX9-iN
1153 (day27) by different current steps (injections) at the current clamp mode (the protocol of
1154 current clamp is shown upper right). (**H**) Example of a mature miR-124+ISX9-iN (day27) that
1155 exhibits spontaneous post-synaptic activity at -70 mV holding potential. Representative
1156 traces of ionic currents induced by application of the neurotransmitter GABA in two different
1157 concentrations (300µM and 1mM) obtained from a miR-124+ISX9-iN in the early stage of
1158 neuronal maturation (day22) **(I)** and the neurotransmitter glutamate in two different
1159 concentrations (100µM and 300µM) obtained from a miR-124+ISX9-In in the late stage of
1160 maturation (day27) **(J)**.The cell membrane potential was held at -70 mV and the time of
1161 agonist application is indicated in bars above the traces. **(K)** Superimposed traces obtained
1162 from a mature miR-124+ISX9-iN (day 26) with application of 100 µM glutamate (Glut) or co-

application of 100µM Glut+CNQX indicated that the antagonist CNQX inhibits the AMPA/ kainate glutamate receptor.

Figure 4: RNA-Seq analysis revealed both independent and cooperative transcriptional contributions of miR-124 and ISX9 in the reprogramming process

(A) Heat map analysis of 300 up- and down-regulated DEGs that belong to the GO terms: Glial cell differentiation, Gliogenesis, Astrocyte development, Generation of neurons, Neuron differentiation, Regulation of neuron differentiation, Neurotransmitter transport and Synaptic signaling. **(B)** GO analysis of biological processes for the up-regulated DEGs in miR-124-iNs vs astro (in orange) and miR-124+ISX9-iNs vs astro (in red). **(C)** GO analysis of biological processes for the down-regulated DEGs in miR-124-iNs vs astro. GO terms are ranked according to $\log_{10}$FDR and the intensity legends indicate the fold enrichment of each GO term. **(D)** Heat map analysis of 54 up-regulated differentially expressed TFs clustered according to the brain region they are developmentally expressed (telencephalon, retina, midbrain and hindbrain). **(E)** Heat map analysis of 40 up- and down-regulated RBPs.

Figure 5: The RNA-binding protein Zfp36l1 is a novel direct target of miR-124

(A) Venn diagram of the miR-124 targets, derived from AGO-HITS-CLIP and the down-regulated DEGs of miR-124 vs sc-miRNA astro RNA-Seq data ($\log_2$(fold change)≤-1, FDR<0.01). Identified miR-124 targets were combined with a public reference list of genes, expressed in astrocytes, resulting in a set of 130 genes. **(B)** miR-124 direct binding to the 3' UTR of *Zfp36l1* and *ZFP36L1*, in mouse and human species respectively. miR-124 binds with perfect seed complementarity (7mer-M8 site) in both species. **(C)** RT-qPCR validation of the mRNA levels of miR-124 direct target *Zfp36l1* at day7 (average ± SD, n=3 independent experiments, **p<0.01 and ***p<0.001 vs sc-miRNA). **(D)** GO analysis of biological processes for Zfp36l1 direct targets that are also significantly up-regulated in miR-124-iNs vs sc-miRNA astro. GO terms are ranked according to $\log_{10}$FDR and the intensity legend shows the fold enrichment of each GO term. **(E)** Volcano plot comparing the $\log_2$(fold change) of TPM values in the miR-124-iNs vs sc-miRNA astro condition versus the $\log_{10}$(FDR) values. Significantly up-regulated ($\log_2$(fold change)≥1, FDR<0.05) and down-regulated ($\log_2$(fold change)≤-1, FDR<0.05) genes are shown in green and orange respectively. Labels of Zfp36l1 and neuronal-specific up-regulated genes that are also Zfp36l1 direct targets are portrayed. **(F)** RT-qPCR validation of the mRNA levels of the Zfp36l1 targets *Elavl4, Nova1, Rbofox1, Rcor2* and *Tox* at day7 (average ± SD, n=3 independent experiments, *p<0.05, **p<0.01 and ***p<0.001 versus sc-miRNA).

1195 **Figure 6: Targeting of Zfp36l1 by miR-124 plays a key role in the miR-124-induced cell fate**
1196 **switch of astrocytes to iNs**

1197 **(A)** Schematic representation of the TSB binding region in the 3'UTR of *Zfp36l1* mRNA. **(B)**
1198 Western blot analysis of the protein levels of Zfp36l1 in the absence or presence of increasing
1199 concentrations of TSB (miR-124:TSB molecular ratio 4:1 and 2:1) at day5 of the
1200 reprogramming protocol. Actin protein levels have been used as loading control for
1201 normalization of Zfp36l1 protein levels. Normalized Zfp36l1 protein levels in sc-miRNA
1202 transfected astrocytes have been set to 1 and the fold change of normalized Zfp36l1 protein
1203 levels of each condition vs sc-miRNA is presented in the box below. **(C)** RT-qPCR analysis of
1204 the mRNA levels of the Zfp36l1 targets *Tox, Rbfox1, Nova1, Rcor2* and *Elavl4* in the presence
1205 or absence of increasing concentrations of TSB (miR-124:TSB molecular ratio 4:1, 2:1 and 1:1)
1206 at day3 of the reprogramming protocol (average ± SD, n=3 independent
1207 experiments,*p<0.05, **p<0.01 and ***p<0.001 versus sc-miRNA and $^{\#}$p<0.05, $^{\#\#}$p<0.01
1208 versus miR-124). (**D**) Immunostaining of astrocytes reprogrammed with miR-124 or miR-124
1209 along with increasing concentrations of TSB (4:1 and 2:1) with anti-Tuj1 antibody at day5 of
1210 the reprogramming protocol. **(E)** Quantification of the percentage of Tuj1+ cells at day5
1211 (average ±SD, n=3 independent experiments *p<0.05 and **p<0.01 versus miR-124). **(F)**
1212 Morphological characterization of Tuj1+ cells at day5. Quantification of the percentages of
1213 multipolar Tuj1+ cells (3 or more processes extending from soma), Tuj1+ cells with 1-2
1214 processes and Tuj1+ cells with an astrocyte-like morphology (rectangular soma with none or
1215 1-2 processes) (average ± SD, n=3 independent experiments, **p<0.01 versus miR-124). **(G)**
1216 Proposed model of independent and cooperative transcriptional and post-transcriptional
1217 contributions of miR-124 and ISX9 in miR-124/ISX9–induced direct neuronal conversion of
1218 cortical astrocytes: miR-124 represses astrocytic identity by down-regulating many astrocytic
1219 genes and directly targeting the RBP Zfp36l1, leading to the up-regulation of the direct
1220 Zfp36l1 targets and TFs *Tox* and *Rcor2*. Tox is known to up-regulate the cortical IP marker and
1221 TF *Tbr2* (Artegiani et al. 2015), which is also further up-regulated by ISX9, along with the
1222 neurogenic TFs *Neurog2* and *NeuroD1*. Additionally, miR-124-induced down-regulation of
1223 *Zfp36l1* results in the up-regulation of the neuronal-specific RBPs *Nova1* and *Rbfox1*, the
1224 latter being further strongly up-regulated by ISX9. These RBPs along with the strongly up-
1225 regulated nElavl RBPs *Elavl2, Elavl3* and *Elavl4* by ISX9 contribute to the stabilization and
1226 efficient translation of many neuronal mRNAs (J. A. Lee et al. 2016; Scheckel et al. 2016;
1227 Weyn-Vanhentenryck et al. 2014). Finally ISX9 transcriptionally up-regulates many neuronal
1228 maturation genes leading to the functional maturation of miR-124+ISX9-iNs. Post-

1229 transcriptional events and the RBPs are highlighted in blue, transcriptional events along with
1230 the TFs are shown in green, while down-regulated genes and (blocked) inhibitory mechanisms
1231 are shown in grey, (dashed lines present knowledge from the literature).

1232 **Figure 7: miR-124 induces reprogramming of resident reactive astrocytes to iNs with deep-**
1233 **layer cortical identity *in vivo* following cortical trauma**

1234 **(A)** Experimental setup. **(B)** LV-124-transduced cells in the peritraumatic cortical parenchyma
1235 expressing the mature neuronal marker NeuN, 3 weeks after viral transduction. Inset area
1236 indicated in white frame. Scale bar 50µm. **(C)** Percentage of control LV-GFP and LV-124
1237 transduced cells expressing the mature neuronal marker NeuN, 6 days and 3 weeks post-
1238 transduction with or without treatment with ISX9. LV-GFP 6 days vs 3 weeks: p=0.104, LV-124
1239 6 days vs 3 weeks: p**=0.00116, LV-124 6 days vs LV-124-ISX9 3 weeks: p**=0.00104, LV-GFP
1240 3 weeks vs LV-124 3 weeks: p**=0.0036, LV-GFP 3 weeks vs LV-124-ISX9 3 weeks:
1241 p**=0.00337, LV-124 3 weeks vs LV-124-ISX9 3 weeks: p=0.8427, n=4 for all groups and time
1242 points. **(D)** LV-miR-124-transduced cells in the peritraumatic cortical parenchyma expressing
1243 the deep layer cortical neuronal marker Tbr1 3 weeks after viral transduction. Image from an
1244 animal transduced with LV-miR-124 and co-treated with ISX9. Inset area indicated in white
1245 frame. White arrows indicate NeuN+/Tbr1+ transduced cells. Scale bar 50µm. **(E)** Percentage
1246 of LV-124-transduced cells expressing Tbr1, 3 weeks post-transduction with or without
1247 treatment with ISX9. LV-124 3 weeks vs LV-124-ISX9 3 weeks: p=0.1503, n=4 for both groups.

1248

1249

1250

1251

1252

1253

1254

1255

1256

1257 **Table 1:** Sequences of primers for real-time PCR used in this study

Gene	Forward primer	Reverse primer
Mash1	TCTCCGGTCTCGTCCTACTC	CAAAGTCCATTCCCAGGAGA
Neurog2	GTCCCCATACAGCTGCACTT	CAGGTGAGGTGCATAACGGT
Tbr2	CACCCAGAATCTCCTAACACTG	AGCCTCGGTTGGTATTTGTG
Tbr1	TCCAGACGTTCACTTTTCCG	CCCGTGTAGATCGTGTCATAG
Cux1	AGCAGAGACTTTAAGGGAACAG	GCAGCCAACTCTACTTCTAGG
Fezf2	TTTGTGGCAAAGGCTTTCAC	TCTTGTCGTTGTGGGTGTG
Gsx2	GATTCCACTGCCTCTCCATG	CGGGACAGGTACATATTGGAAG
Dlx1	CAGTTCCGTGCAGTCCTAC	ATTGTCCTGGGTTTACGGATC
Sox4	GAACGCCTTTATGGTGTGGT	GAACGGAATCTTGTCGCTGT
Sox11	CCCTGTCGCTGGTGGATAAG	GGTCGGAGAAGTTCGCCTC
Hes6	TACCGAGGTGCAGGCCAA	AGTTCAGCTGAGACAGTGGC
NeuroD1	TTGAAGCCATGAATGCAGAG	TCTTGGGCTTTTGATCATCC
Scrt1	AATCATGCCCAGGTCCTTC	CCACGTAGTCACTGAGGTATC
Lhx6	GACACCATGATCGAGAACCTC	CAATTGCTCTGCGGTGAAG
Chd5	ATCTACGAAATCTGGCACCG	CCCTTGTGGATCTCAGACTTG
En1	CTACTCATGGGTTCGGCTAAC	TCTTTAGCTTCCTGGTGCG
Foxa1	AGGGTTGGATGGTTGTGTC	AGGCCGGAGTTCATGTTG
Lmx1b	CGGGATCGGAAACTGTACTG	AGCAGAAACAGCCCAAGTG
Hoxc4	CAAGCAACCCATAGTCTACCC	AACTCTTTCTCTAATTCCAGGACC
Phox2a	TCCCTTCTCTGGAGTTCTGTC	GATAATGCCAGGTCCAGAAGG
Elavl2	AATAACAGGGCAGAGCTTGG	TCTGATTGAGGCTGAGCTTG
Elavl3	GGTTCGGGATAAGATCACAGG	CAGAACTGGGACGTGCATAG
Elavl4	AGAATCCTGCAAACTCGTGAG	ATGGTTTTGGTCTGGAGTCTG
Nova1	GCTGGCTACCTCTGGATCAT	TGGGATGCCATTTAGCTTGC
Zfp36l1	CACACCAGATCCTAGTCCTTG	CTGGGAGTGCTGTAGTTGAG
Zfp36	TCTCTTCACCAAGGCCATTC	GAGTCCGAGTTTATGTTCCAAAG
Rbpj	TCCCAAAACCCGGATAACC	TTTCGCATAGCTTCCCTAGTG
Tcf7l1	CTACAGCAACGACCACTTCTC	GGTAATACGGTGACAGCTCAG

Tcf4	CACAAACCATTACAGCACCTC	GTGTGGTCAGGAGAATAGATCG
Nfic	GGACGGAAGACATAGAAGGAG	GGGCTGTTGAATGGAGATTTG
Tox	TGCTCTCCAATTCCATCTCTG	CTGTCTGATGTCTGTAGGCTG
Rcor2	GCATGTACCTGAGTCCTGAAG	CTGCTATTGGTCTGCTTCATG
Rbfox1	AGTTACGGACGAGTTTATGCTG	AGAGAACGAGACCCACATCA

1258

Figure 1

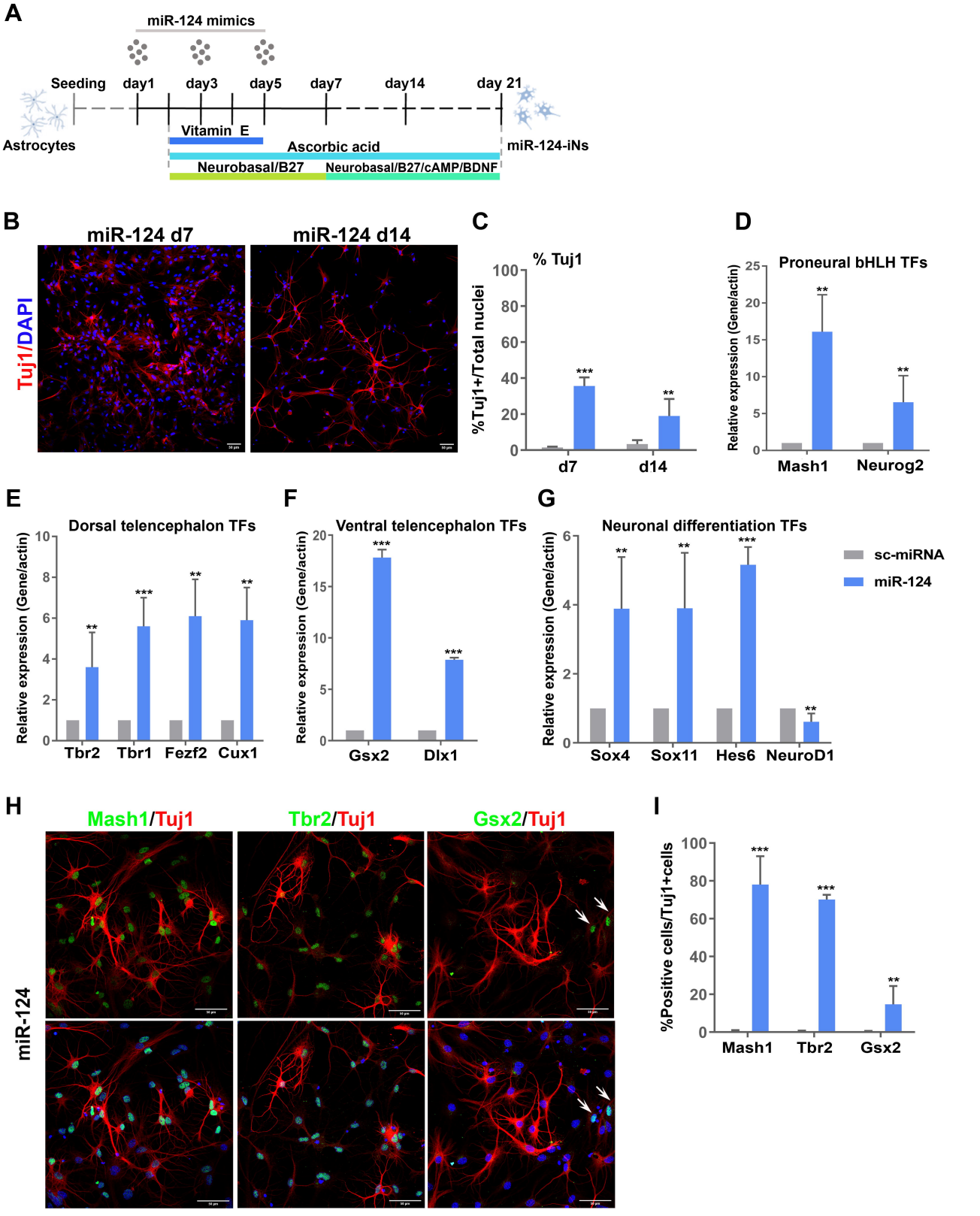
A
miR-124 mimics
Seeding
day1
day3
day5
day7
day14
day 21
Astrocytes
Vitamin E
Ascorbic acid
miR-124-iNs
Neurobasal/B27
Neurobasal/B27/cAMP/BDNF
B
miR-124 d7
miR-124 d14
Tuj1/DAPI
C
% Tuj1
%Tuj1+/Total nuclei
d7
d14
D
Proneural bHLH TFs
Relative expression (Gene/actin)
Mash1
Neurog2
E
Dorsal telencephalon TFs
Relative expression (Gene/actin)
Tbr2
Tbr1
Fezf2
Cux1
F
Ventral telencephalon TFs
Relative expression (Gene/actin)
Gsx2
Dlx1
G
Neuronal differentiation TFs
Relative expression (Gene/actin)
Sox4
Sox11
Hes6
NeuroD1
sc-miRNA
miR-124
H
Mash1/Tuj1
Tbr2/Tuj1
Gsx2/Tuj1
miR-124
I
%Positive cells/Tuj1+cells
Mash1
Tbr2
Gsx2

Figure 2

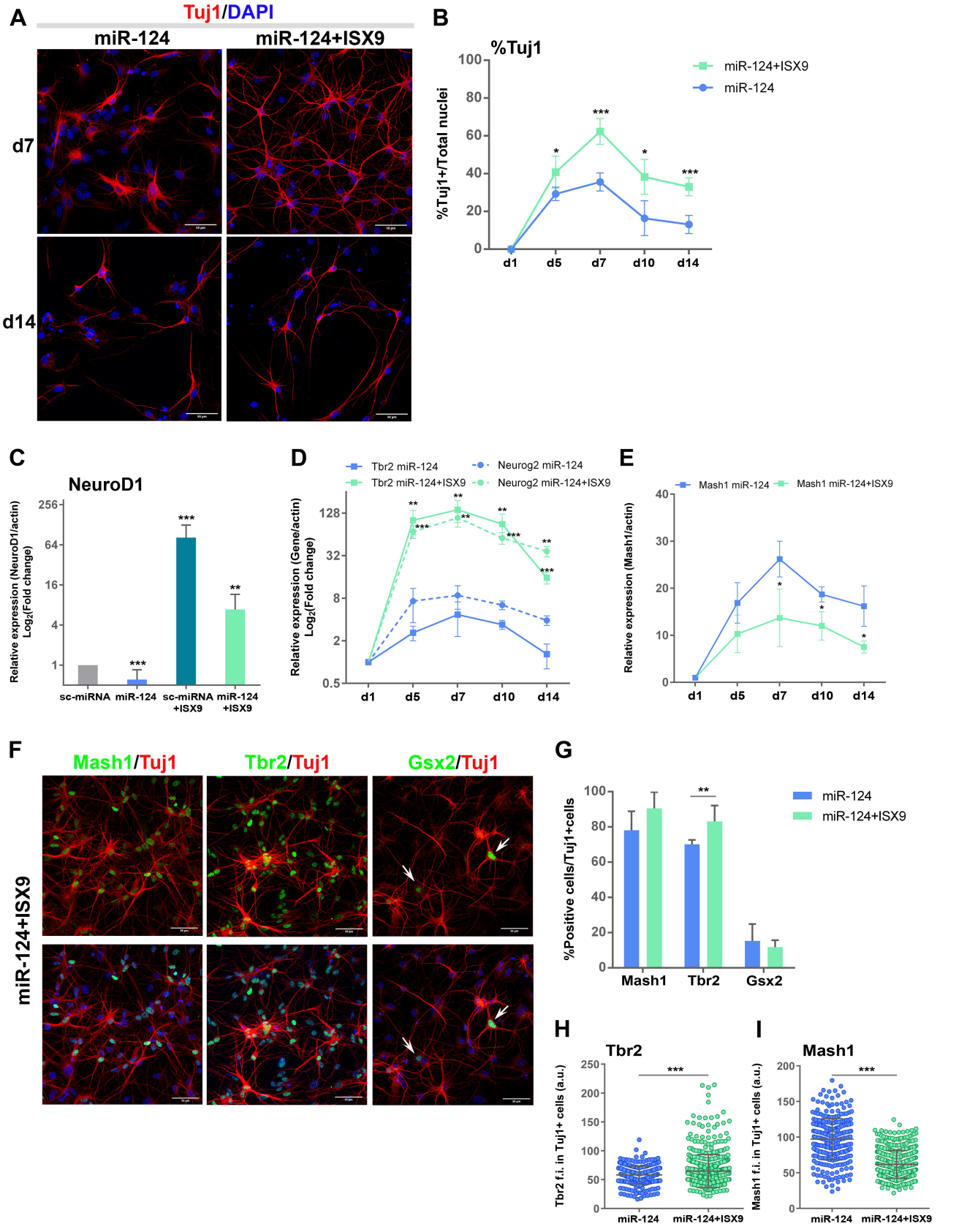
A
Tuj1/DAPI
miR-124
miR-124+ISX9
d7
d14
B
%Tuj1
%Tuj1+/Total nuclei
miR-124+ISX9
miR-124
d1
d5
d7
d10
d14
C
NeuroD1
Relative expression (NeuroD1/actin)
Log2(Fold change)
sc-miRNA
miR-124
sc-miRNA +ISX9
miR-124 +ISX9
D
Tbr2 miR-124
Tbr2 miR-124+ISX9
Neurog2 miR-124
Neurog2 miR-124+ISX9
Relative expression (Gene/actin)
Log2(Fold change)
E
Mash1 miR-124
Mash1 miR-124+ISX9
Relative expression (Mash1/actin)
F
Mash1/Tuj1
Tbr2/Tuj1
Gsx2/Tuj1
miR-124+ISX9
G
%Positive cells/Tuj1+cells
miR-124
miR-124+ISX9
Mash1
Tbr2
Gsx2
H
Tbr2
Tbr2 f.i. in Tuj1+ cells (a.u.)
miR-124
miR-124+ISX9
I
Mash1
Mash1 f.i. in Tuj1+ cells (a.u.)
miR-124
miR-124+ISX9

Figure 3

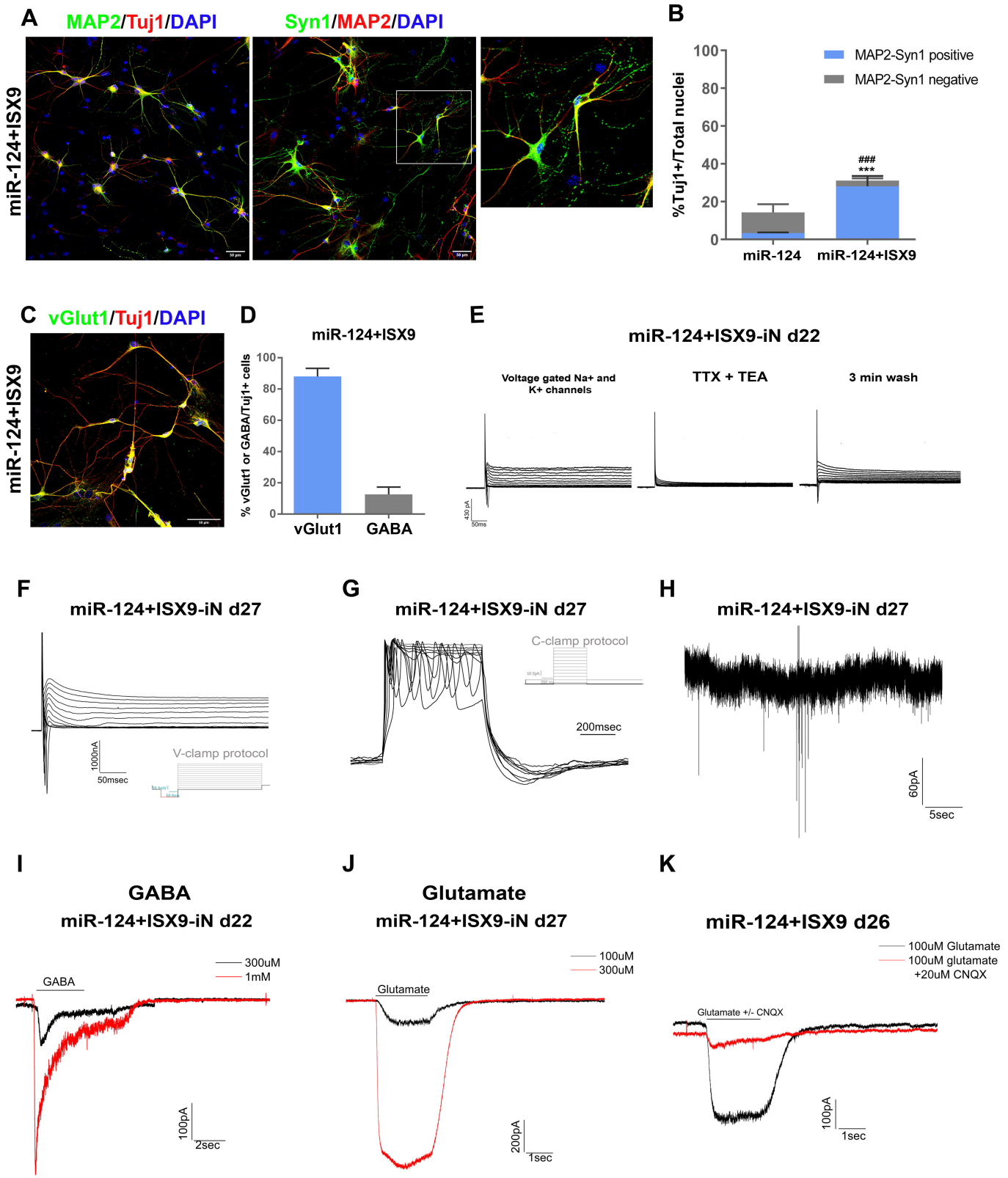
A
MAP2/Tuj1/DAPI
Syn1/MAP2/DAPI
miR-124+ISX9
B
MAP2-Syn1 positive
MAP2-Syn1 negative
%Tuj1+/Total nuclei
100
80
60
40
20
0
###
***
miR-124
miR-124+ISX9
C
vGlut1/Tuj1/DAPI
miR-124+ISX9
D
miR-124+ISX9
% vGlut1 or GABA/Tuj1+ cells
100
80
60
40
20
0
vGlut1
GABA
E
miR-124+ISX9-iN d22
Voltage gated Na+ and K+ channels
TTX + TEA
3 min wash
430 pA
50ms
F
miR-124+ISX9-iN d27
1000nA
50msec
V-clamp protocol
G
miR-124+ISX9-iN d27
C-clamp protocol
200msec
H
miR-124+ISX9-iN d27
60pA
5sec
I
GABA
miR-124+ISX9-iN d22
300uM
1mM
GABA
100pA
2sec
J
Glutamate
miR-124+ISX9-iN d27
100uM
300uM
Glutamate
200pA
1sec
K
miR-124+ISX9 d26
100uM Glutamate
100uM glutamate +20uM CNQX
Glutamate +/- CNQX
100pA
1sec

Figure 4

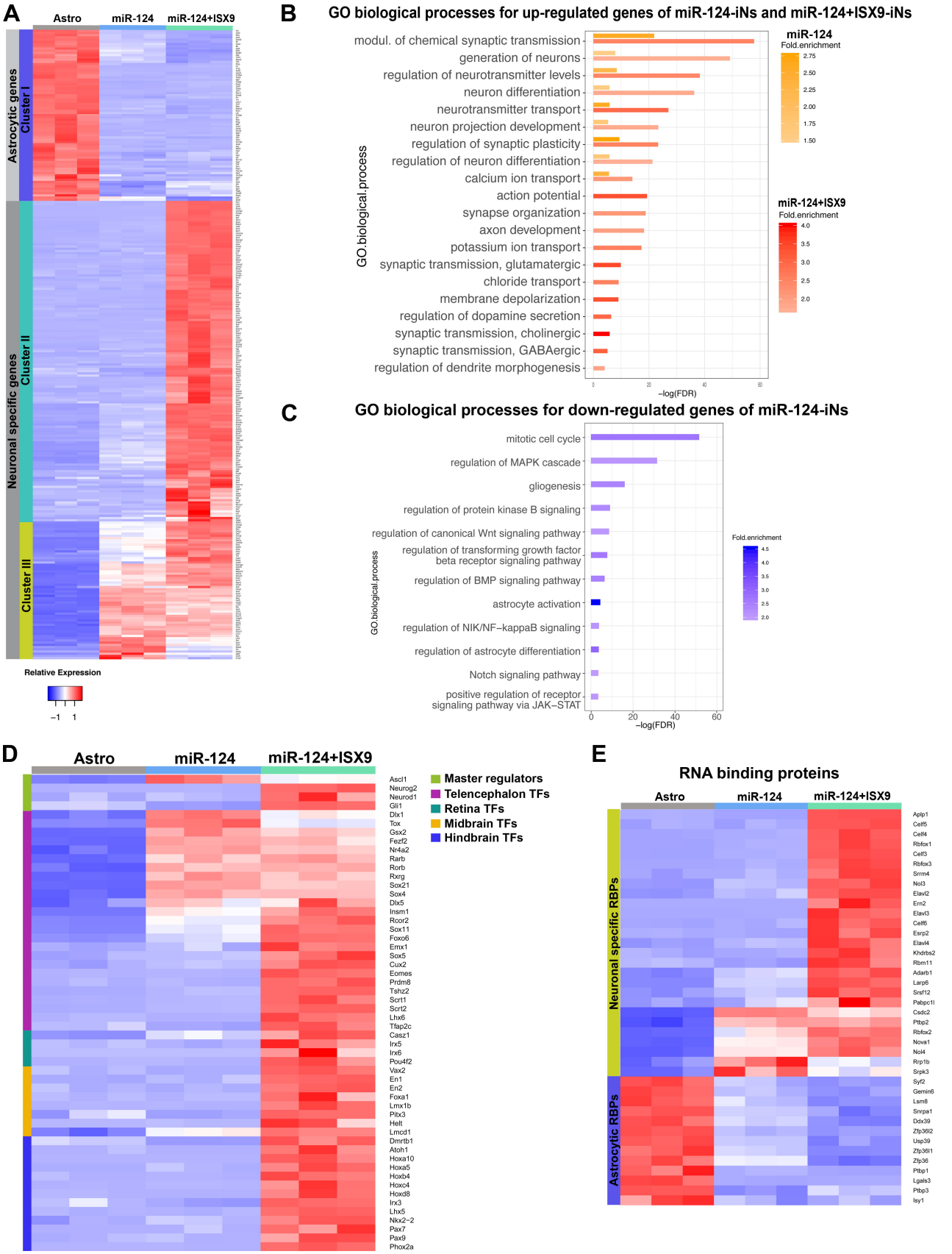
A
Astro
miR-124
miR-124+ISX9
Astrocytic genes
Cluster I
Neuronal specific genes
Cluster II
Cluster III
Relative Expression
−1
1
B
GO biological processes for up-regulated genes of miR-124-iNs and miR-124+ISX9-iNs
modul. of chemical synaptic transmission
generation of neurons
regulation of neurotransmitter levels
neuron differentiation
neurotransmitter transport
neuron projection development
regulation of synaptic plasticity
regulation of neuron differentiation
calcium ion transport
action potential
synapse organization
axon development
potassium ion transport
synaptic transmission, glutamatergic
chloride transport
membrane depolarization
regulation of dopamine secretion
synaptic transmission, cholinergic
synaptic transmission, GABAergic
regulation of dendrite morphogenesis
GO.biological.process
−log(FDR)
miR-124
Fold.enrichment
miR-124+ISX9
Fold.enrichment
C
GO biological processes for down-regulated genes of miR-124-iNs
mitotic cell cycle
regulation of MAPK cascade
gliogenesis
regulation of protein kinase B signaling
regulation of canonical Wnt signaling pathway
regulation of transforming growth factor beta receptor signaling pathway
regulation of BMP signaling pathway
astrocyte activation
regulation of NIK/NF−kappaB signaling
regulation of astrocyte differentiation
Notch signaling pathway
positive regulation of receptor signaling pathway via JAK−STAT
GO.biological.process
−log(FDR)
Fold.enrichment
D
Astro
miR-124
miR-124+ISX9
Master regulators
Telencephalon TFs
Retina TFs
Midbrain TFs
Hindbrain TFs
Ascl1
Neurog2
Neurod1
Gli1
Dlx1
Tox
Gsx2
Fezf2
Nr4a2
Rarb
Rorb
Rxrg
Sox21
Sox4
Dlx5
Insm1
Rcor2
Sox11
Foxo6
Emx1
Sox5
Cux2
Eomes
Prdm8
Tshz2
Scrt1
Scrt2
Lhx6
Tfap2c
Casz1
Irx5
Irx6
Pou4f2
Vax2
En1
En2
Foxa1
Lmx1b
Pitx3
Helt
Lmcd1
Dmrtb1
Atoh1
Hoxa10
Hoxa5
Hoxb4
Hoxc4
Hoxd8
Irx3
Lhx5
Nkx2−2
Pax7
Pax9
Phox2a
E
RNA binding proteins
Astro
miR-124
miR-124+ISX9
Neuronal specific RBPs
Astrocytic RBPs
Aplp1
Celf5
Celf4
Rbfox1
Celf3
Rbfox3
Srrm4
Nol3
Elavl2
Ern2
Elavl3
Celf6
Esrp2
Elavl4
Khdrbs2
Rbm11
Adarb1
Larp6
Srsf12
Pabpc1l
Csdc2
Ptbp2
Rbfox2
Nova1
Nol4
Rrp1b
Srpk3
Syf2
Gemin6
Lsm8
Snrpa1
Ddx39
Zfp36l2
Usp39
Zfp36l1
Zfp36
Ptbp1
Lgals3
Ptbp3
Isy1

Figure 5

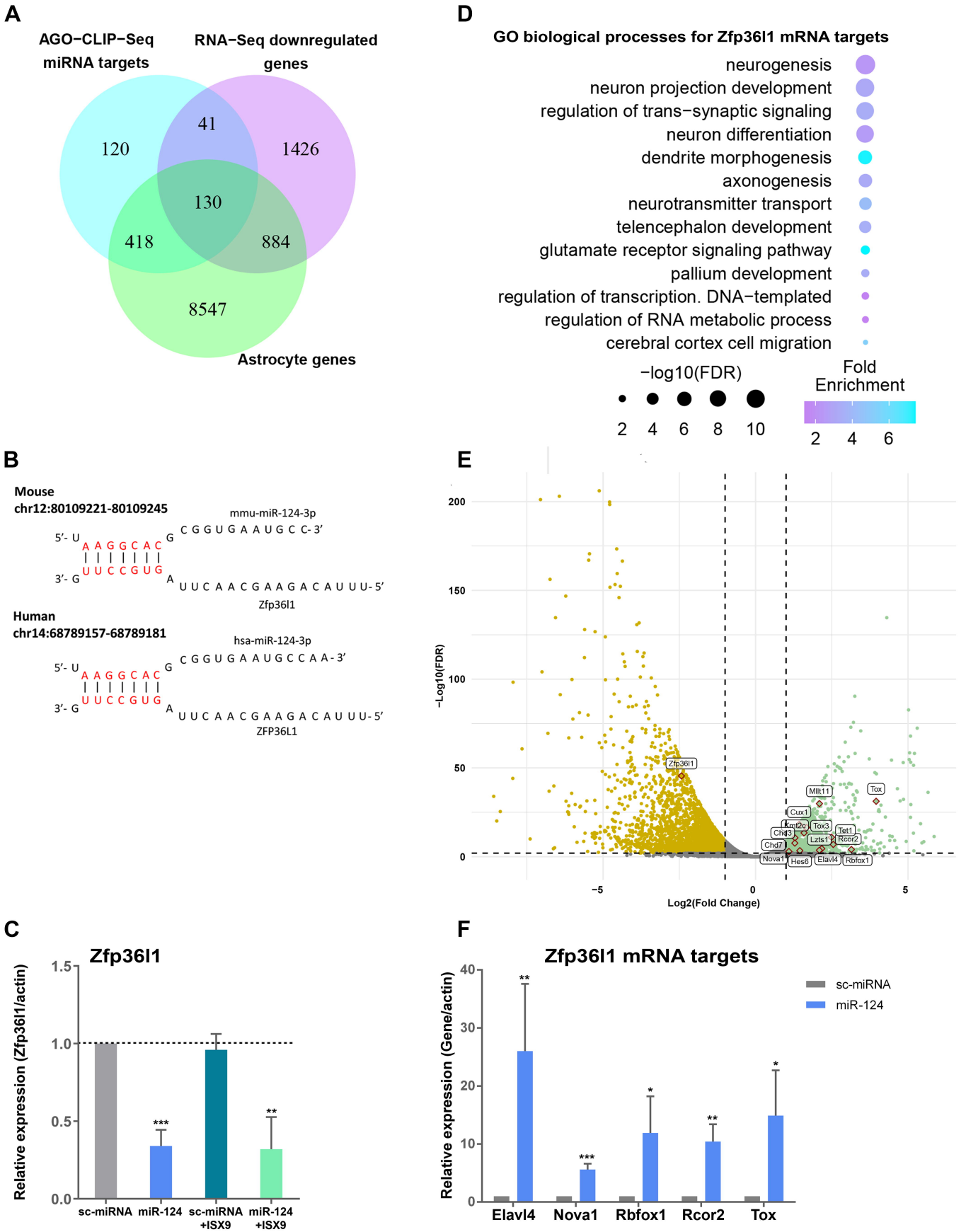
A
AGO−CLIP−Seq miRNA targets
RNA−Seq downregulated genes
Astrocyte genes
120
41
1426
130
418
884
8547
B
Mouse
chr12:80109221-80109245
mmu-miR-124-3p
5′- U
3′- G
A A G G C A C
U U C C G U G
G
A
C G G U G A A U G C C- 3′
U U C A A C G A A G A C A U U U- 5′
Zfp36l1
Human
chr14:68789157-68789181
hsa-miR-124-3p
5′- U
3′- G
A A G G C A C
U U C C G U G
G
A
C G G U G A A U G C C A A- 3′
U U C A A C G A A G A C A U U U- 5′
ZFP36L1
C
Zfp36l1
Relative expression (Zfp36l1/actin)
1.5
1.0
0.5
0.0
***
**
sc-miRNA
miR-124
sc-miRNA +ISX9
miR-124 +ISX9
D
GO biological processes for Zfp36l1 mRNA targets
neurogenesis
neuron projection development
regulation of trans−synaptic signaling
neuron differentiation
dendrite morphogenesis
axonogenesis
neurotransmitter transport
telencephalon development
glutamate receptor signaling pathway
pallium development
regulation of transcription. DNA−templated
regulation of RNA metabolic process
cerebral cortex cell migration
−log10(FDR)
2 4 6 8 10
Fold Enrichment
2 4 6
E
−Log10(FDR)
200
150
100
50
0
Zfp36l1
Mllt11
Tox
Cux1
Kmt2c
Tox3
Chd3
Tet1
Lzts1
Rcor2
Chd7
Nova1
Hes6
Elavl4
Rbfox1
−5
0
5
Log2(Fold Change)
F
Zfp36l1 mRNA targets
Relative expression (Gene/actin)
40
30
20
10
0
sc-miRNA
miR-124
**
***
*
**
*
Elavl4
Nova1
Rbfox1
Rcor2
Tox

Figure 6

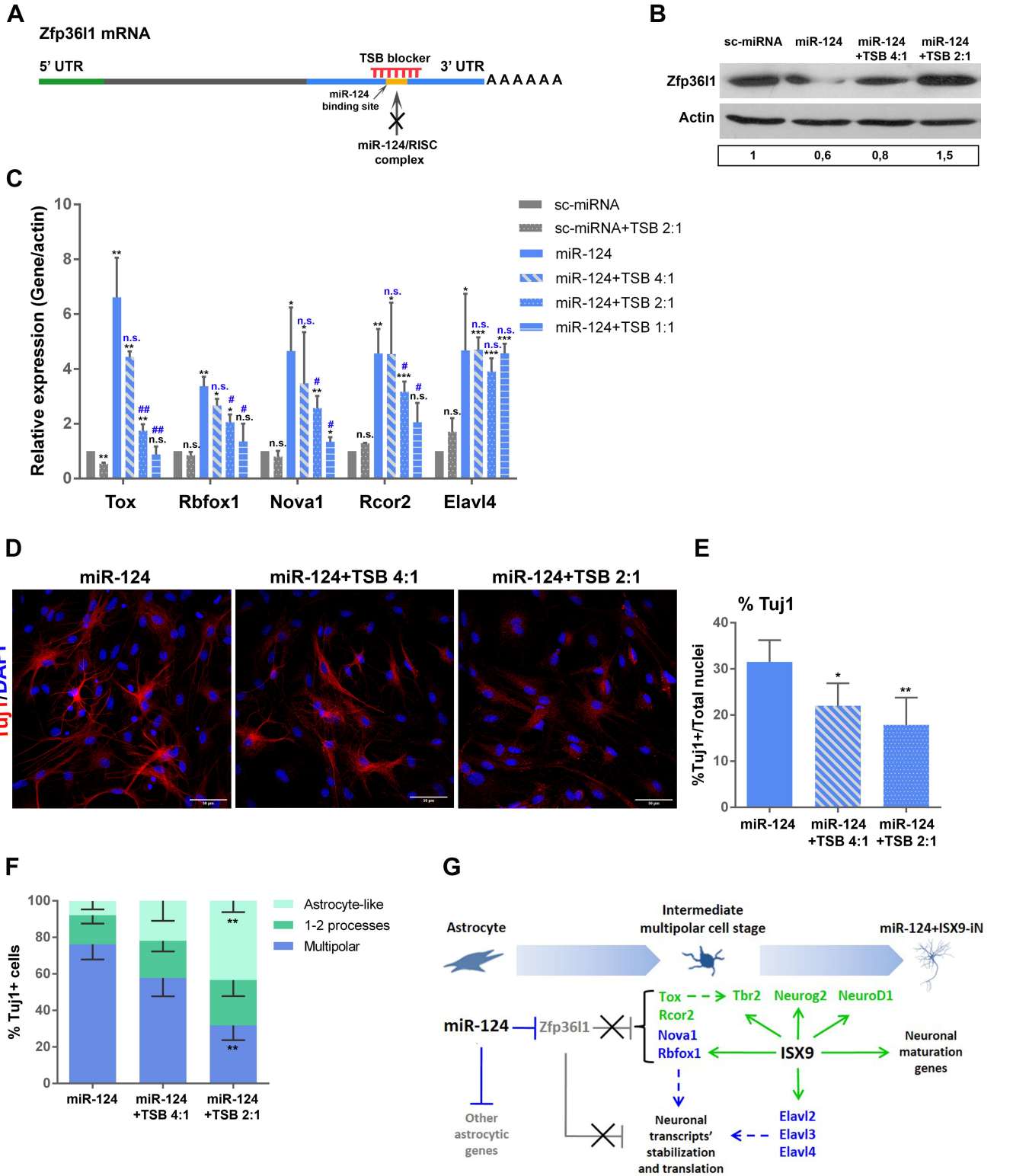
A
Zfp36l1 mRNA
5' UTR
TSB blocker
3' UTR
A A A A A A
miR-124 binding site
miR-124/RISC complex
B
sc-miRNA
miR-124
miR-124 +TSB 4:1
miR-124 +TSB 2:1
Zfp36l1
Actin
1
0,6
0,8
1,5
C
Relative expression (Gene/actin)
sc-miRNA
sc-miRNA+TSB 2:1
miR-124
miR-124+TSB 4:1
miR-124+TSB 2:1
miR-124+TSB 1:1
Tox
Rbfox1
Nova1
Rcor2
Elavl4
D
miR-124
miR-124+TSB 4:1
miR-124+TSB 2:1
Tuj1/DAPI
E
% Tuj1
%Tuj1+/Total nuclei
miR-124
miR-124 +TSB 4:1
miR-124 +TSB 2:1
F
% Tuj1+ cells
Astrocyte-like
1-2 processes
Multipolar
miR-124
miR-124 +TSB 4:1
miR-124 +TSB 2:1
G
Astrocyte
Intermediate multipolar cell stage
miR-124+ISX9-iN
miR-124
Zfp36l1
Tox
Rcor2
Nova1
Rbfox1
Tbr2
Neurog2
NeuroD1
ISX9
Neuronal maturation genes
Other astrocytic genes
Neuronal transcripts' stabilization and translation
Elavl2
Elavl3
Elavl4

Figure 7

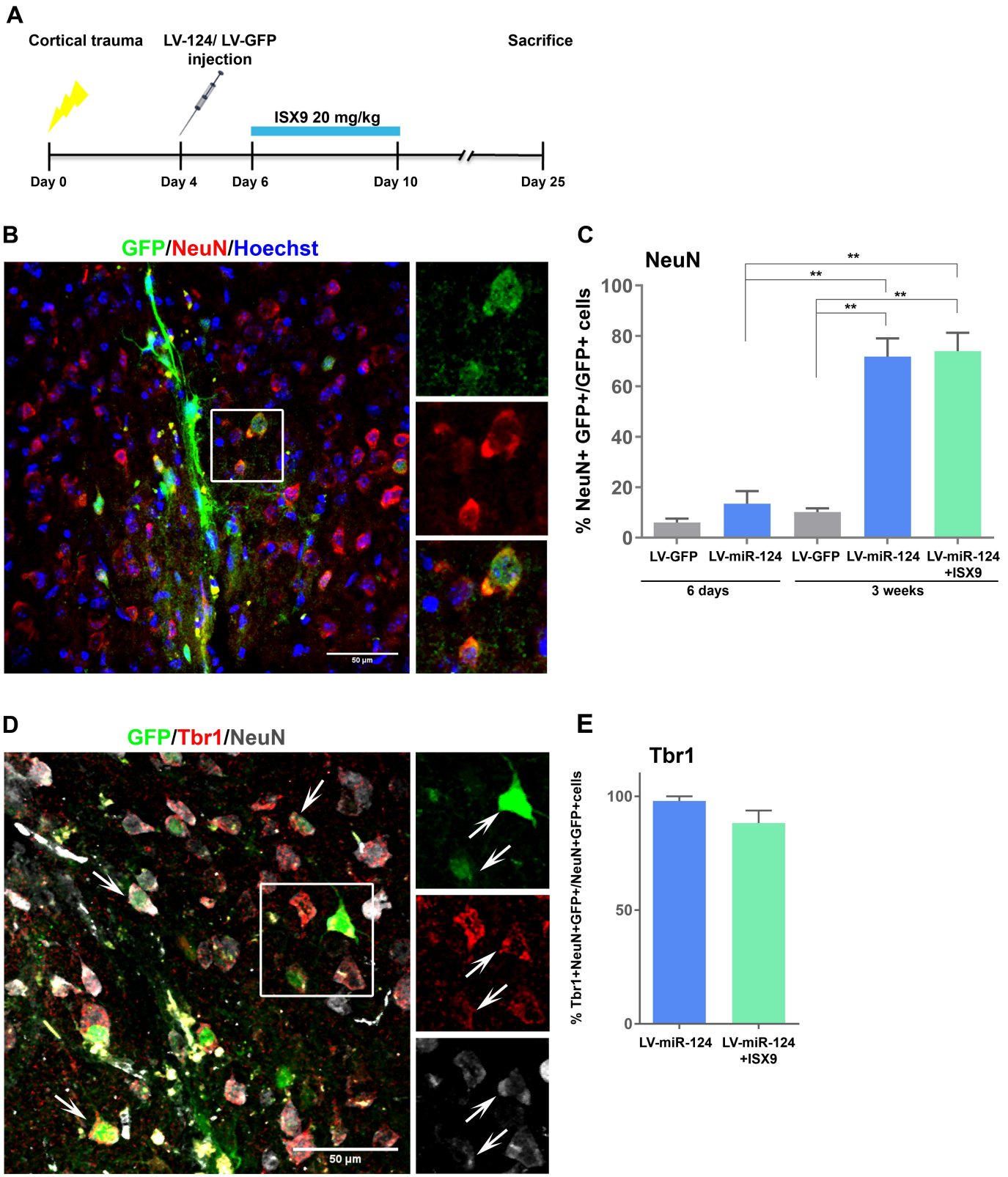
A
Cortical trauma
LV-124/ LV-GFP injection
Sacrifice
ISX9 20 mg/kg
Day 0
Day 4
Day 6
Day 10
Day 25
B
GFP/NeuN/Hoechst
50 µm
C
NeuN
% NeuN+ GFP+/GFP+ cells
100
80
60
40
20
0
**
**
**
**
LV-GFP
LV-miR-124
LV-GFP
LV-miR-124
LV-miR-124 +ISX9
6 days
3 weeks
D
GFP/Tbr1/NeuN
50 µm
E
Tbr1
% Tbr1+NeuN+GFP+/NeuN+GFP+cells
100
50
0
LV-miR-124
LV-miR-124 +ISX9